Vortex pinning by natural linear defects in thin films of YBa2Cu3O7-¿.

Klaassen, F.C.; Doornbos, G.; Huijbregtse, J.M.; van der Geest, R.C.F.; Dam, B.; Griessen, R.P.

document version
Publisher's PDF, also known as Version of record

Link to publication in VU Research Portal

citation for published version (APA)
Klaassen, F. C., Doornbos, G., Huijbregtse, J. M., van der Geest, R. C. F., Dam, B., & Griessen, R. P. (2001). Vortex pinning by natural linear defects in thin films of YBa2Cu3O7-¿. *Physical Review B. Condensed Matter and Materials Physics*, *64*, 184523.

Vortex pinning by natural linear defects in thin films of YBa$_2$Cu$_3$O$_{7-\delta}$

F. C. Klaassen, G. Doornbos, J. M. Huijbregtse, R. C. F. van der Geest, B. Dam, and R. Griessen
Faculty of Sciences, Division of Physics and Astronomy, Vrije Universiteit, De Boelelaan 1081, 1081 HV Amsterdam, The Netherlands
(Received 1 February 2001; published 25 October 2001)

The behavior of the superconducting current density $j_s(B,T)$ and the dynamical relaxation rate $Q(B,T)$ of YBa$_2$Cu$_3$O$_{7-\delta}$ thin films exhibits a number of features typical for strong pinning of vortices by growth induced linear defects. At low magnetic fields $j_s(B)$ and $Q(B)$ are constant up to a characteristic field B^*, that is directly proportional to the linear defect density n_{disl}. The pinning energy $U_c(B=0)\approx 600$ K can be explained by half-loop excitations determining the thermal activation of vortices at low magnetic fields. Extending the Bose glass theory [D. R. Nelson and V. M. Vinokur, Phys. Rev. B **48**, 13 060 (1993)], we derive a different expression for the vortex pinning potential $\varepsilon_r(R)$, which is valid for all defect sizes and describes its renormalization due to thermal fluctuations. With this expression we explain the temperature dependence of the true critical current density $j_c(0,T)$ and of the pinning energy $U_c(0,T)$ at low magnetic fields. At high magnetic fields $\mu_0 H \gg B^*$ the current density experiences a power law behavior $j_s(B) \sim B^\alpha$, with $\alpha \approx -0.58$ for films with low n_{disl} and $\alpha \approx -0.8$ to -1.1 for films with high n_{disl}. The pinning energy in this regime, $U_c(\text{high } B) \approx 60-200$ K is independent of magnetic field, but depends on the dislocation density. This implies that vortex pinning is still largely determined by the linear defects, even when the vortex density is much larger than the linear defect density. Our results show that natural linear defects in thin films form an analogous system to columnar tracks in irradiated samples. There are, however, three essential differences: (i) typical matching fields are at least one order of magnitude smaller, (ii) linear defects are smaller than columnar tracks, and (iii) the distribution of natural linear defects is nonrandom, whereas columnar tracks are randomly distributed. Nevertheless the Bose glass theory, that has successfully described many properties of pinning by columnar tracks, can be applied also to thin films. A better understanding of pinning in thin films is thus useful to put the properties of irradiated samples in a broader perspective.

I. INTRODUCTION

In high-T_c superconducting YBa$_2$Cu$_3$O$_{7-\delta}$ thin films, very high critical currents up to 10^{12} A m^{-2} are observed. This is roughly two orders of magnitude higher than in high quality single crystals, and comparable to the depairing current j_0. These current densities indicate that a large amount of *correlated* defects is present in thin films, providing for strong vortex pinning.[1] In single crystals vortices are only weakly pinned by randomly distributed point defects. Strong vortex pinning is an important aspect for high-T_c applications, but the nature of the defect responsible for the observed large current densities in thin films remained unresolved for a long time. Many different defects can act as a strong pinning source:[2] twin boundaries,[3] (low angle) grain boundaries,[4] large extended precipitates[5] or oxygen vacancies,[6] surface roughness,[7,8] and (screw) dislocations.[6,9–12] The effect of grain boundaries was studied on films grown on bicrystal substrates,[13,14] while the effect of antiphase boundaries was studied on films grown on miscut substrates.[15] Other groups sought ways to explain j_c by *artificially* introducing various types of defects, such as columnar defects,[16–18] antidots[19,20] or (magnetic) impurities.[21–25] Most studies are based on samples with an *artificially induced* defect structure, by using doping or heavy ion irradiation, or specially chosen (miscut, bicrystal) substrates in order to study various pinning mechanisms. However, the reason for the near to perfect pinning properties, i.e., $j_c \simeq j_0$ of high quality *as-grown* films remained unexplained for a long time.

The most extensively studied method to increase the critical current density, especially of single crystals, is the irradiation by heavy ions.[26] The columnar tracks with diameter $D \sim 50-100$ Å that are formed constitute effective linear pinning centers. As a result the critical current increases by more than one order of magnitude, while the irreversibility line shifts to higher fields. This behavior can be understood within the Bose glass theory.[27] However, even after heavy ion radiation the critical current of single crystals is still considerably lower than in thin films. Moreover, in YBa$_2$Cu$_3$O$_{7-\delta}$ thin films, where the critical current density is already close to the depairing current (up to $j_c \approx 0.25 j_0$ at $T=4.2$ K), the introduction of artificial defects proved to be less effective, since j_s is increased by typically a factor 2–5 at low temperatures, depending on the type of irradiation.[28–30] Only at temperatures close to T_c the effect is larger due to the shift of the irreversibility line.

In order to identify the mechanism responsible for strong pinning in *as-grown* thin films it is essential to analyze systematically and quantitatively the intrinsic pinning properties in connection with the defect structure. In an early attempt to relate the critical current to the number of dislocations, growth spirals were taken as a measure for the number of natural linear defects.[9,10,31] However, as the formation of spirals is a growth kinetic process, screw dislocations do not always form growth spirals. This is evident from pulsed laser deposited (PLD) YBa$_2$Cu$_3$O$_{7-\delta}$ films, which always have high critical currents although the formation of growth spirals is usually prohibited by the growth conditions.[32] Moreover, edge dislocations pin vortices equally well, as was

shown by Diaz *et al.*,[14] who considered vortex pinning by a low angle grain boundary consisting of a dense row of edge dislocations. This indicates that the as-grown surface morphology is not a proper measure for the linear defect density.

As an alternative model, Mezzetti *et al.*[33] relate pinning in thin $YBa_2Cu_3O_{7-\delta}$ films to the island structure of the films. It is assumed that the islands are separated by planar defects situated in the trenches between the islands. Planar defects, for example low angle grain boundaries or (hidden) weak links, can have strong pinning properties. They can be effectively described as a network of Josephson junctions, where the critical current of each junction is given by a Fraunhofer-like expression.[13] Mezzetti *et al.* fit the measured magnetic field dependence of the critical current density $j_s(B)$ to a distribution in the length of these Josephson junctions. Their approach fits the experimentally observed current density $j_s(B)$ well at intermediate temperatures, but no proof is given of the actual existence of such a network of planar defects in thin $YBa_2Cu_3O_{7-\delta}$ films. Moreover, this model does not explain the temperature dependence of j_s and B^* nor the field dependence at low ($T<0.3T_c$) temperatures.

Recently[34] we developed a technique to determine the linear defect density n_{disl} of both screw and edge dislocations in thin $YBa_2Cu_3O_{7-\delta}$ films. We proved that upon wet chemical etching in a 1% Br in ethanol solution both type of dislocations form etch pits. Measuring the superconducting current density $j_s(B)$ at $T=4.2$ K, we find a plateau below a characteristic field B^*. The size of this plateau is directly proportional to the dislocation density n_{disl} with a proportionality constant $0.7\Phi_0$. From this we conclude that, at low magnetic fields, dislocations are the most important pinning source in thin $YBa_2Cu_3O_{7-\delta}$ films, and that every defect can pin one vortex.

In this paper we present a systematic study on the behavior of the superconducting current density $j_s(B,T)$ and the magnetic relaxation $Q(B,T)$ in $YBa_2Cu_3O_{7-\delta}$ films. We demonstrate the existence of a matching effect in the relaxation, similar to that in $j_s(B)$. The magnitude of the zero field pinning energy we measured, $U_c(B=0)\approx 600$ K, suggests that half-loop excitations are the elementary vortex excitations in thin films at low magnetic fields. Moreover, it appears that far above B^* the critical current is still determined by (collective) strong pinning due to linear defects. We focus on the behavior at low temperatures $T\lesssim 70$ K, since at higher temperatures the true critical current density j_c cannot be easily related to the measured superconducting current density j_s. Moreover, at temperatures close to T_c the vortex glass transition and the melting transition have already been investigated extensively by many groups.[35–37]

The paper is organized as follows. In Sec. II we describe the main theoretical concepts used to explain our results. Section III is devoted to the preparation of the films and to a description of the experimental techniques. In Sec. IV we present the general features of $YBa_2Cu_3O_{7-\delta}$ films, in terms of the current density j_s, the relaxation rate Q, and the pinning energy U_c. Section V is devoted to a discussion mainly in terms of the Bose glass theory. We explain the observed temperature dependence of $j_c(B=0,T)$ and $U_c(T)$ and we show that for small defects thermal fluctuations lead to a

stronger renormalization of the pinning potential than was assumed before. This could explain the strong decrease of $B^*(T)$ with temperature, both in thin films and in irradiated crystals. In Sec. VI we summarize our results and give an overview of the remaining questions.

II. THEORY

In single crystals the pinning and dynamics of vortices is described by the theory of weak collective pinning.[38,39] A single vortex is pinned by many pinning centers, that are randomly distributed and have a random pinning force. The vortex tries to increase its pinning energy by taking advantage of as many pinning centers as possible, and secondly a vortex wants to remain straight in order to minimize its elastic energy. As a result of this competition between pinning and elastic energy, the vortex breaks up in correlated pieces of length L_c, the correlation length. This picture works very well in describing the situation in single crystals of high-T_c superconductors, but it is not appropriate for strong pinning. Particularly, it cannot explain the plateau like features in $j_c(B)$ observed in thin films at low magnetic fields, nor the strong magnetic field dependence of $j_c(B)$ at high magnetic fields. In the case of strong pinning, vortices are pinned over their full length by an extended defect, that locally suppresses the superconducting order parameter. The Bose glass theory[27] has successfully described the strong pinning results of irradiated single crystals. We will show that the same theory can also be applied to describe pinning by natural linear defects in thin films. The essential parameter in this description is the ratio $x \equiv r_r/\sqrt{2}\xi$ between the radius of a linear defect r_r and the vortex core $\sqrt{2}\xi$. In thin films both quantities are comparable in size, which complicates the description appreciably.

A. Strong pinning by linear defects

The irradiation of single crystals or films with heavy ions creates columnar tracks where the crystal structure is heavily distorted, causing a suppression of the superconducting order parameter. Also the core of a dislocation in thin films is characterized by a strong deformation of the crystal lattice and a corresponding suppression of the order parameter. Mkrtchyan and Shmidt[40] calculated the pinning properties of a cylindrical hole in a superconductor, which provides an accurate description for large linear defects $x \gg 1$. Nelson and Vinokur[27,41] observed that the problem of linear defect pinning is analogous to the quantum problem of interacting bosons in two dimensions, trapped in a static random potential. Due to this analogy many properties of the vortex system can be derived easily and this so-called Bose glass theory gives an accurate description of strong pinning by columnar or linear defects. In this section we describe the main aspects of the Bose glass theory, that are relevant for vortex pinning in thin films. We mainly follow the description used by Blatter *et al.*,[42] which is completely analogous to the original paper by Nelson and Vinokur.[27] In the next section we derive a general formula for the pinning potential $\varepsilon_r(R)$, which is valid when $x \approx 1$ as well.

The starting point in the Bose glass theory is, that at low magnetic fields a single vortex is strongly pinned by a linear (columnar) defect. The vortices can freely accommodate to the lattice of pinning sites until the shear energy exceeds the pinning energy per unit length ε_r. Then a crossover to a collective pinning regime occurs at the crossover or accommodation field:[43]

$$B^* \approx 4(\varepsilon_r/\varepsilon_0)B_\Phi, \qquad (1)$$

with $\varepsilon_0 = \Phi_0^2/4\pi\mu_0\lambda^2$ a characteristic vortex energy per unit length and $B_\Phi \equiv n_{disl}\Phi_0$ is the matching field, at which the vortex density exactly equals the defect density.

Experimentally, the matching field B_Φ can be determined unambiguously from the irradiation dose or, in the case of dislocation pinning in thin films, by counting the number of etchpits.[44] The accommodation field is determined by the interaction between the vortex lattice and the defect lattice. In thin films it marks the end of a plateau in the critical current density. The size of the plateau is determined either by using an empirical fit of $j_s(B)$,[34] or the simple criterion $j_s(B^*)/j_s(0) = 0.9$.[33] In this paper we use the term characteristic field for B^*, as in Ref. 34, to denote the fitted size of the plateau of $j_s(B)$. In irradiated single crystals a plateau has not been observed. Instead B^* has been defined as the field that marks the transition of the field dependence of the critical current from an exponential decrease towards $j_s(B) \propto 1/B$. Alternatively, a similar value for $B^*(T)$ was derived from the maximum in $d\ln j_s/dT|_B$.[45] The absence of a plateau in j_s is attributed to strong vortex-vortex interactions at the matching field (note that the typical distance between the columnar tracks $d_r \approx 20$–50 nm$\ll\lambda$). In this films vortex-vortex interactions are less important at the matching field, because the linear defects in films are much further apart $d_r \gtrsim \lambda$.

In the limit of very large, $x \gg 1$, and very small defects, $x \ll 1$, the pinning potential yields[42]

$$\varepsilon_r(R) = \frac{\varepsilon_0}{2}\ln\left(1 - \frac{r_r^2}{R^2}\right) \quad \text{for } x \gg 1, \qquad (2)$$

$$\varepsilon_r(R) = -\frac{\varepsilon_0}{2}\frac{r_r^2}{R^2 + 2\xi^2} \quad \text{for } x \ll 1, \qquad (3)$$

with R the distance of the vortex from the center of the pinning site. The critical current density j_c is determined by the balance between the Lorentz force and the maximum pinning force $-d\varepsilon_r/dR|_{max}$. Since the pinning potential diverges in Eq. (2) at $R = r_r$, a cutoff of $\varepsilon_r(R) \simeq \ln(r_r/\sqrt{2}\xi)$ was introduced to determine j_c for large defects, giving $f_{pin} \approx \varepsilon_r/\sqrt{2}\xi$. The critical current density is now

$$j_c = \frac{3\sqrt{3}}{4\sqrt{2}}j_0 \simeq j_0, \quad \text{for } x \gg 1, \qquad (4)$$

$$j_c = \frac{27\sqrt{2}}{64}\left(\frac{r_r}{2\xi(T)}\right)^2 j_0, \quad \text{for } x \ll 1. \qquad (5)$$

B. The pinning potential $\varepsilon_r(R)$ for $x \approx 1$

When the vortex core and the defect size are comparable, the solutions, given by Eqs. (2) and (3), are not applicable. The expressions (2) and (3) connect only for $R \to \infty$, i.e., when the vortex is far away from the linear defect, whereas for $R \lesssim r_r$, i.e., when the vortex is pinned in the defect, both equations deviate strongly. Note, that since the coherence length $\xi(T)$ increases with temperature, there is always a crossover in behavior from $x > 1$ to $x < 1$. In thin films the defect core is typically of the order of a few Burgers vectors, which would give $r_r \approx 2$–3 nm for screw dislocations, somewhat larger than $\xi(0)$. This shows that a general equation is needed, which is valid not only for very large or very small defects, but also when $x \approx 1$. This is in fact also true for columnar tracks, that have a radius $r_r \simeq 3$–5 nm not much larger than the coherence length.

To obtain the pinning potential for all defect sizes we calculate how much the order parameter is reduced at the position of the defect. For a vortex which has its center at a position R from the center of the defect, put at the origin of the coordinate system, the pinning potential is

$$\varepsilon_r(R) = -\frac{1}{2}\mu_0 H_c^2 \int\int [1 - |\Psi(|\mathbf{r}-\mathbf{R}|)|^2]r\,dr\,d\vartheta, \qquad (6)$$

with $|\Psi(|\mathbf{r}-\mathbf{R}|)|^2$ the size of the superconducting order parameter at a point (r, ϑ), and the integration done over the full defect. Taking for the vortex core $\Psi(|\mathbf{r}-\mathbf{R}|) = \Psi(R')$ $= f(R')\exp[i\varphi]$, with $f(R') = R'/(R'^2 + 2\xi^2)^{1/2}$ (from Ref. 46), we obtain (see Appendix A for a derivation)

$$\varepsilon_r(R) = -\frac{\varepsilon_0}{2}\left\{\left[\frac{1}{2}\left(\frac{\sqrt{2}\xi}{|R|}\right)\frac{(r_r^2 - R^2 + 2\xi^2)}{2\xi^2}\right] \right.$$
$$\left. -\left[\frac{1}{2}\left(\frac{\sqrt{2}\xi}{|R|}\right)\frac{(-R^2 + 2\xi^2)}{2\xi^2}\right]\right\}. \qquad (7)$$

The depth of the pinning potential at $R = 0$ is given by

$$\varepsilon_r(0) \approx -\frac{\varepsilon_0}{2}\ln\left[1 + \frac{r_r^2}{2\xi^2}\right] = -\frac{\varepsilon_0}{2}\ln[1 + x^2]. \qquad (8)$$

Note that Eq. (8) is exactly the interpolation formula, proposed by Nelson and Vinokur. In Fig. 1 the pinning potentials according to Eq. (7) are drawn for $r_r = 2\xi$ and $r_r = \xi$, together with their Taylor's expansion to lowest order, and the results for large and small x, given by Eqs. (2) and (3). In the limit of large R Eq. (7) correctly approaches the theoretical results derived in Refs. 40 and 39. The depth of the potential, Eq. (8), is smaller than in Eqs. (2) and (3) when $r_r \approx \xi$, but for very small and very large x it correctly approaches Eq. (3) and the cutoff of Eq. (2).

C. Temperature effects

There are two effects that determine the temperature dependence of $j_c(T)$. The first is an intrinsic temperature dependence, due to the parameters $\lambda(T)$ and $\xi(T)$. Equations (4) and (5) directly lead to
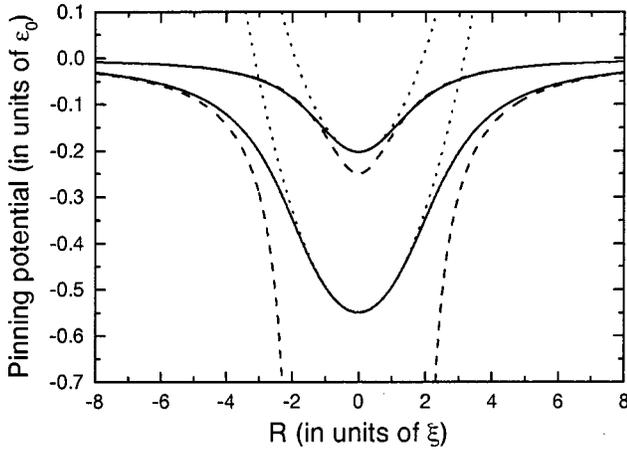
FIG. 1. Vortex-pinning potentials for $r_r = 2\xi$ and $r_r = \xi$. Solid lines are the true pinning potentials, given by Eq. (7). Dashed lines are the theoretical calculations for large defects, by Mkrtchyan and Shmidt (Ref. 40) and for small defects, by Blatter *et al.* (Ref. 39). Dotted lines denote the lowest order Taylor's expansion Eq. (11), which is used to calculate the effect of thermal fluctuations.

$$j_c(T) \approx 1/(\lambda^2(T)\xi^\nu(T)), \qquad (9)$$

with $\nu = 1$ and $\nu = 3$ for large and small defects, respectively. For the real pinning potential, Eq. (7), one can show that the maximum pinning force $f_{max} = -d\varepsilon_r/dR|_{max} \approx -d\varepsilon_r/dR|_{R=r_r}$. The relative error in this approximation $\Delta f_{max}/f_{max}$ is less than 4% for $x > 0.6$, and using this approximation we find for the critical current density

$$j_c(T) \approx \frac{\varepsilon_0}{2\Phi_0\xi} \frac{1}{r_r} \left(\frac{r_r^2 + \xi^2}{\sqrt{2r_r^2 + \xi^2}} - \xi \right)$$

$$= \frac{3\sqrt{3}}{8} \left(\frac{r_r^2 + \xi^2}{r_r\sqrt{2r_r^2 + \xi^2}} - \frac{\xi}{r_r} \right) j_0(T). \qquad (10)$$

Note that the prefactor before $j_0(T)$ is an increasing function of r_r, which means that the maximum pinning force increases with increasing defect size. Equation (10) is not a convenient expression, but it can be fitted to $j_c(T) \sim 1/(\lambda^2(T)\xi^\nu(T))$, with ν a fit parameter ranging from $\nu = 1$ to $\nu = 3$, depending on the defect size. In other words Eq. (9), describing $j_c(T)$ for very large or very small defects, can be used generally for all defect sizes, with ν reflecting the crossover from very large ($x \gg 1$, $\nu = 1$) to very small defects ($x \ll 1$, $\nu = 3$).

The second effect influencing $j_c(T)$ are thermal fluctuations. Due to the confinement of the vortices onto the their pinning sites, the loss of entropy reduces the effective pinning depth of the pinning potential. The influence of thermal (entropic) fluctuations was calculated by taking a square well of depth $\tilde{\varepsilon}_r$ and extension $b_0 \equiv \max(r, \sqrt{2}\xi)$ as the vortex pin potential,[42] giving for the pinning energy per unit length $\varepsilon_r(T) \simeq \tilde{\varepsilon}_r((1 - (T/\tilde{T}_{dp}^r)^2)$ for low temperatures, where $\tilde{\varepsilon}_r$ is the depth of the pinning potential without thermal fluctuations, and $\tilde{T}_{dp}^r \equiv b_0\sqrt{\varepsilon_l\varepsilon_r}$ is the depinning energy (for convenience we have omitted the Boltzmann constant k_B). Note

that the depinning *energy* is temperature dependent itself, $\tilde{T}_{dp}^r(T) \sim 1/\lambda^2(T)$, and we have $\tilde{T}_{dp}^r(T_{dp}) \equiv T_{dp}$, with T_{dp} the depinning *temperature*. For very large defects it is reasonable to approach $\varepsilon_r(R)$, given by Eq. (2), with a square well potential, but in general the form of the pinning potential is different. To calculate the effect of thermal fluctuations at low temperatures we use the Taylor's expansion of Eq. (7) to lowest order, i.e.,

$$\varepsilon_r(R) \approx \varepsilon_r(R=0) + \frac{\varepsilon_0}{2} \frac{r_r^2}{(r_r^2 + 2\xi^2)^2} R^2, \qquad (11)$$

which is a harmonic oscillator potential. From the eigenvalues of the harmonic oscillator and the correct boson-vortex mapping (see Appendix B for a derivation), we obtain

$$\varepsilon_r(T) \simeq \tilde{\varepsilon}_r(1 - T/\tilde{T}_{dp}^r) \quad \text{at low } T. \qquad (12)$$

The thermal fluctuation factor is now linear in $T/\tilde{T}_{dp}^r$, indicating that thermal fluctuations have a stronger effect on the pinning potential than was assumed in the Bose glass theory. An estimate for the depinning energy at zero temperature, taking $\varepsilon_l = \varepsilon_r = 0.2\varepsilon_0$ and $b_0 = r_r = 2\xi$, yields $\tilde{T}_{dp}^r \approx 400$ K $\gg T_c$. This indicates, that at low temperatures $T < 0.5T_c$ the effect of thermal fluctuations in thin $YBa_2Cu_3O_{7-\delta}$ films will not be very large, although the strong temperature dependence of $B^*(T)$ could indicate that $\tilde{T}_{dp}^r(0)$ is lower (see the discussion in Sec. V B). Upon approaching the depinning *temperature* T_{dp} the depinning *energy* $\tilde{T}_{dp}^r(T) \sim 1/\lambda^2(T)$ decreases quickly and thermal fluctuations reduce the effective pinning strength considerably.

III. EXPERIMENT

A. Sample preparation

$YBa_2Cu_3O_{7-\delta}$ thin films were deposited by means of pulsed laser deposition (PLD) on (100) $SrTiO_3$ substrates.[47] The PLD system consists of a KrF excimer laser (wavelength 248 nm, pulse time 30 ns, frequency 5 Hz) and a UHV system in combination with projection optics to ensure a stoichiometric deposition from the $YBa_2Cu_3O_{7-\delta}$ target. By using different substrate temperatures during deposition between $T_{sub} \approx 700\,°C$ and $T_{sub} \approx 850\,°C$ we are able to tune reproducibly the island size of the films between $D = 80$ nm to $D = 500$ nm.[44] The films are all c-axis oriented and have a thickness of $d \approx 140$ nm. XRD analysis shows a good overall crystallinity of all films. The c axis of the films $c = 11.68(3)$ Å is very close to the single crystal value of 11.677 Å, while the (005) rocking curve full width at half maximum $\Delta\omega_{(005)} \lesssim 0.1°$. The average transition temperature T_c, measured resistively using a four point method, $T_c = 90.4$ K with a standard deviation of 0.4 K and a typical transition width $\Delta T_c \lesssim 0.5$ K.[48] To determine the defect structure *and* the pinning properties of the same film, we cut each film into four pieces. For critical current measurements one piece was patterned by standard UV photolithography into a ring of typically 3–5 mm in diameter and 125–500 μm width. In this geometry we can safely assume a well

TABLE I. General properties of pulsed laser deposited (PLD) and sputtered $YBa_2Cu_3O_{7-\delta}$ films on $SrTiO_3$ investigated in this work. d is the film thickness, T_c the transition temperature (not measured for all films), ΔT_c the width of the transition, n_{disl} the dislocation density, and d_r the average defect spacing.

Film	Deposition method	d (nm)	T_c (K)	ΔT_c (K)	n_{disl} (μm^{-2})	d_r (nm)
$A67$	dc sputtering	192	90.6	0.6	7	378
$B670$	PLD	110	90.4	0.6	28	189
$C496$	PLD	140	90.6	0.3	34	171
$D203$	PLD	140	91		57	132
$E493$	PLD	70	89.7	0.4	72	118
$F554$	PLD	140			90	105

defined current distribution and relaxation rate, which we confirmed by magneto-optical measurements.[49] The other pieces were used for microstructural analysis, such as AFM, XRD, and wet chemical etching to determine the linear defect density (see the next section).

For comparison we measured a 70 nm thin film ($E493$) and a film ($A67$), prepared by means of dc sputtering. The latter was sputtered at $T=840$ °C and 3 mbar oxygen pressure with a substrate-target distance of 2 cm. After deposition the film was postannealed for 1 h at 650 °C in 10^3 mbar O_2 in order to optimize the superconducting properties. In this way, films containing large growth spirals are obtained, forming island sizes up to $D=2$ μm.[50]

In Table I an overview is given about the deposition and structural details of all films treated in this paper.

B. Defect structure

The surface morphology of the films is studied by a tapping mode AFM, using a Nanoscope IIIa. In Fig. 2 an AFM
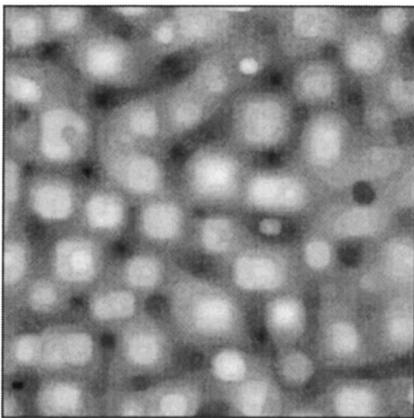

FIG. 2. 1.5×1.5 μm^2 surface topography of a 140 nm thick $YBa_2Cu_3O_{7-\delta}$ film (film $C496$), obtained by atomic force microscopy. The island structure can be clearly distinguished. The average island diameter is $D=200$ nm. The dislocations are mainly situated in the trenches around the islands (Ref. 44). As a result their distribution is not random in the sense that the nearest neighbor distance exhibits a relatively small variation. Vertical scale: black-white ~40 nm.

image is shown of film $C496$. Characteristic for all laser ablated films is the island structure, with an island diameter of typically 100–500 nm, separated by deep trenches (up to 20% of the film thickness). By means of wet chemical etching in a 1.0 vol % Br-ethanol solution we obtain the linear defect density n_{disl} from the density of etch pits. By etching a very short time, the etch pits are visible together with the as-grown, not yet erased island structure. Most linear defects are situated in the trenches resulting in a linear relationship between the island density and the linear defect density, with on average one linear defect per island.[44] From the radial distribution function of the etch pits, we see that the defects are nonrandomly distributed, with almost no defects close to each other. As the defect density in films remains constant with thickness, we learn that the dislocations are formed at the substrate-film interface and persist up to the surface of the $YBa_2Cu_3O_{7-\delta}$ film, i.e., they thread through the entire film $\|c$ axis.[44]

Previously, we found indications for an antiphase boundary network, due to the c-axis mismatch between $YBa_2Cu_3O_{7-\delta}$ and the $SrTiO_3$ substrate.[51,52] However, recent TEM observations on our films show, that antiphase boundaries are not a general feature in thin films, whereas the island morphology is. Moreover, no grain boundaries or weak links separating the islands were found.[53] Instead our films consist of large well connected islands, and the dislocations found by TEM appear to be screw dislocations. We conclude that the trenches between the growth islands only reflect a reduction of the film thickness and that there is no network of planar defects related to them. Therefore, the model of Mezzetti et al.[33] is not applicable to our films. Note that the defect distance $d_r\approx200$ nm is much larger than the defect radius $r_r\approx1-3$ nm, which makes it impossible to view these dislocations to be correlated in such a way that they form a planar defect. In low angle grain boundaries the array of dislocations is much denser. For example, in the 4° grain boundary $YBa_2Cu_3O_{7-\delta}$ film, investigated by Diaz et al.,[14] the distance between adjacent edge dislocations $d_r\approx5.6$ nm$\lesssim r_r$, which means that the defect core sizes are almost overlapping. Even if all dislocations in our film would be aligned, we find [using the Shockley-Read formula $d_r=|b|/(2\sin(\vartheta/2))$, with $|b|=0.4$ nm the magnitude of the Burgers vector, and $d_r=200$ nm], that the grain boundary angle $\vartheta\approx0.1°$. This is clearly too small to give any noticeable grain boundary effect, for which the minimum angle would be $\vartheta\gtrsim\vartheta_0\approx3-5°$.[54,55] Hence we may safely assume that in our films we are dealing with pinning at *individual* linear defects.

For sputtered films the one to one correspondence between island density and defect density does not hold. The islands are very large and do not show deep trenches. Instead growth spirals are observed, that can be associated with screw dislocations. After etching other dislocations (mostly edge dislocations) are observed as well, which makes the dislocation density relatively large compared to the island size. Nevertheless, in sputtered films the matching effect is still related to the total measured linear defect density n_{disl}.[34]

This proves once more that the linear defect density, and not the island size, determines the size of the low field plateau in the current density.

C. Determination of the superconducting current density and the relaxation

The superconducting current density is measured by means of capacitive torque magnetometry. When we place a superconducting sample in a magnetic field $\mu_0 \mathbf{H}$ under a specific angle and sweep the field with constant sweep rate $\mu_0 (dH/dt)$, superconducting currents are induced in the sample, which set up a magnetic moment $\mathbf{M}$ perpendicular to the plane of the ring. The sample experiences a torque according to

$$\boldsymbol{\tau} = \mu_0 (\mathbf{M} \times \mathbf{H}). \tag{13}$$

We determine the irreversible torque τ_{irr} at a certain magnetic field by taking half the difference between the ascending (τ_+) and the descending (τ_-) branch of a magnetic hysteresis loop $\tau_{\text{irr}} = (\tau_+ - \tau_-)/2$. We assure that the sample is in the fully penetrated state by performing sweeps over a much larger range than the penetration field. Since the current in a thin film is confined to the film plane, we can calculate the irreversible magnetic moment using $M_{\text{irr}} = \tau_{\text{irr}} / (\mu_0 H \sin \vartheta)$. The current density is directly proportional to the magnetic moment, depending only on a geometrical factor. Using the Bean critical state model,[56] we obtain for ring-shaped samples

$$M_{\text{irr}} = (\pi/3) d (r_o^3 - r_i^3) j_s, \tag{14}$$

with d the sample thickness and r_o and r_i the outer and inner radius of the ring, respectively.

The setup consists of a 7 T magnet in a Oxford cryostat that enables us to measure over a temperature range from 1.7 to 300 K. The magnetic field is applied at an angle of $10°$ from the c axis. As this angle is well within the trapping angle for columnar tracks, we can safely assume that the vortices are parallel to the c axis. Moreover, as shown by Brandt,[57] vortices are straight and perpendicular to the surface over a length $l \sim \lambda$, indicating that even without linear defects vortices would be aligned with the c axis over almost the full film thickness. Vortex kink creation at the surface, as proposed by Indenbom *et al.*,[58] does therefore not occur in thin films with thickness $d \lesssim \lambda$.

Douwes *et al.*[6] showed by comparing transport measurements with torque magnetometry, that the applied magnetic field can be scaled to an effective field along the c-axis $\mu_0 H_{\text{eff}} = \mu_0 H_{\text{appl}} \cos \vartheta$, for angles at least up to $\vartheta = 30°$. In our measurements, with $\cos \vartheta = 0.985$, we set thus $\mu_0 H_{\text{eff}} = \mu_0 H_{\text{appl}}$.

The torquemeter consists of two fixed copper plates, and one movable phosphorous-bronze plate. This plate with the sample is mounted 0.5 mm above the fixed plates. It has two U-shaped cuts that enables the plate to slightly rotate when a torque is exerted (see Ref. 51 for a detailed picture). This torque is measured capacitively.[59] For calibration we mount a

copper-wired coil of known dimensions onto the plate, and measure the torque exerted by the coil, as a function of applied current through the coil.

Note that the measured superconducting current density j_s is in general not the true critical current density j_c, i.e., the current density for which the pinning force and Lorentz force are equal. The difference is caused by the relaxation of the vortex lattice due to thermally activated vortex hopping[60] or quantum creep.[61] In $YBa_2Cu_3O_{7-\delta}$ films the relaxation rate is typically a few percent at low magnetic fields and temperatures. This difference between j_s and j_c is a general experimental feature, also encountered in $I-V$ measurements. The electric field associated with the induced current in a ring according to Faraday's law is

$$E(r) = -\frac{\mathfrak{L}(r) d}{2\pi} \frac{\partial j}{\partial t} - \frac{r}{2} \frac{dB}{dt} \propto \frac{dB}{dt}, \tag{15}$$

with $\mathfrak{L}(r)$ the self-inductance of the ring, d the film thickness, and r the radius of the ring. Because $d \ll r$ the term with $\partial j / \partial t$ can be neglected. From Eq. (15) we see that fixing a sweep rate corresponds exactly to choosing a certain voltage criterium as is usually done in $I-V$ measurements to determine j_c. The equivalence of torque and $I-V$ measurements has been confirmed also experimentally.[62]

The relaxation rate is usually determined by measuring the decay of the magnetic moment in time after having stopped a field sweep. The normalized relaxation rate is then defined as

$$S \equiv -\frac{d \ln j_s}{d \ln t}. \tag{16}$$

There are, however, a few drawbacks in using this method to determine the relaxation rate in thin films. First of all the method is time consuming, since the relaxation, especially at low temperatures, is very slow. Secondly, because of the large demagnetization factor of a thin film, the penetration field is small. Therefore a small overshoot at the end of a field sweep causes dramatic changes in the microscopic field and current distribution, thereby making it impossible to relate the measured magnetic moment to the current density, especially at short time scales. Since most of the relaxation takes place in the first few seconds after a field sweep has stopped, this overshoot seriously hampers an accurate measurement of the relaxation in thin films. There is, however, a convenient way of avoiding these problems by making small hysteresis loops around a certain field, with ever decreasing sweep rates. Due to relaxation, the width of the hysteresis loop decreases with decreasing sweep rate, and we obtain the dynamical relaxation rate

$$Q \equiv \frac{d \ln j_s}{d \ln(dB/dt)} \tag{17}$$

by plotting the hysteresis against the sweep rate on a double logarithmic plot. Due to the ring shape of our sample, we obtain a well defined, uniform relaxation rate. It was shown, both experimentally and theoretically, that both conventional
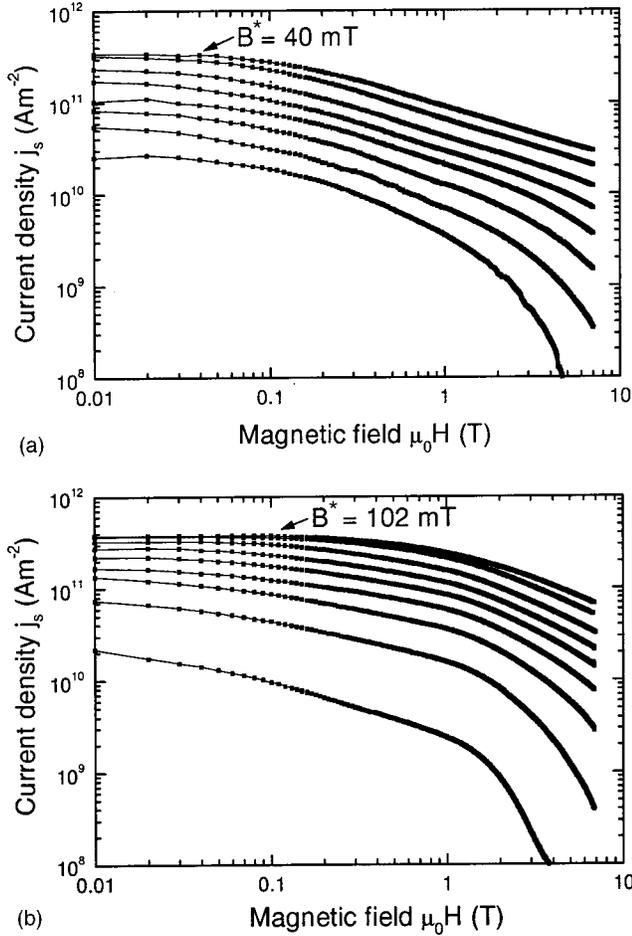
(a)

(b)

FIG. 3. Superconducting current density $j_s(B)$ for two films with different dislocation density; (a) $C496$ with $n_{disl}=34$ μm^{-2} and (b) $E493$ with $n_{disl}=72$ μm^{-2}. From top to bottom $T=4.2$, 10, 20, 30, 40, 50, 60, 70, and 80 K (only $E493$). The arrows indicate the characteristic field at $T=4.2$ K.

and dynamical relaxation measurements essentially yield the same value for the relaxation.[63]

IV. RESULTS

A. General properties of the superconducting current density j_s

The general behavior of the superconducting current density j_s in thin films of YBa$_2$Cu$_3$O$_{7-\delta}$ has a number of distinct features. The most remarkable property is, that at low magnetic fields, the current density $j_s(B)$ exhibits a plateau (Fig. 3 and Ref. 34). Note that this plateau is not an artifact of the logarithmic scale, used for μ_0H; it persist in a linear plot. In Fig. 3 and Fig. 4 we plot $j_s(B,T)$ as a function of magnetic field and temperature respectively, for two films with low and high dislocation density. Comparing many films we typically find that at $T=4.2$ K, $j_s(B=0)\approx(2$ to 6$)$ $\times10^{11}$ A m^{-2}, while at $T=77.5$ K, $j_s=2-4\times10^{10}$ A m^{-2}. These high critical current values confirm, that the films are of excellent quality, like the materials parameters (cf. Sec. III A) already suggested.
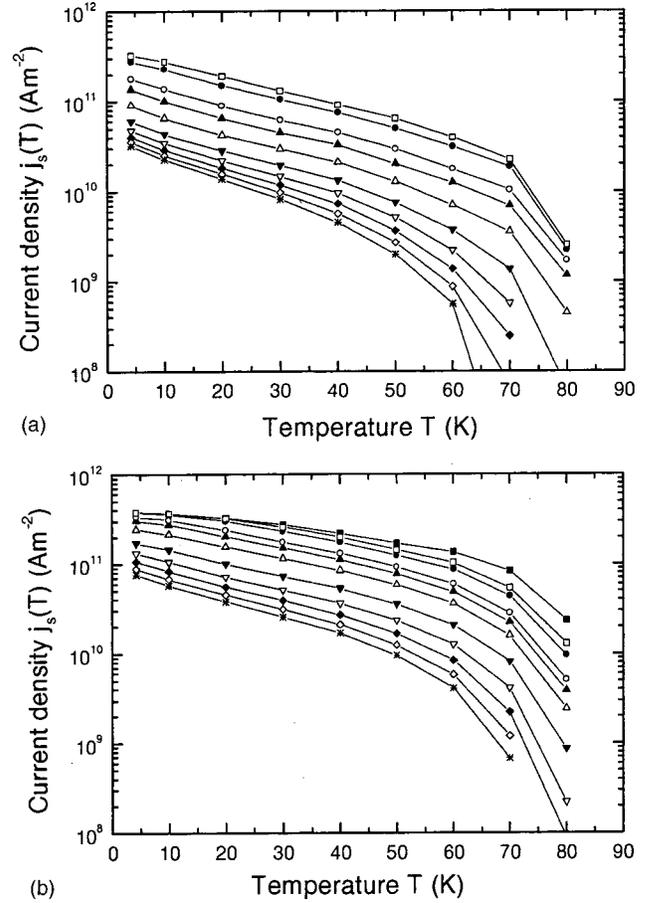

(a)

(b)

FIG. 4. Current density $j_s(T)$ for various magnetic fields of (a) $C496$ and (b) $E493$. From top to bottom $B=0.005$ (■, only $E493$), 0.05 (□), 0.1 (●), 0.3 (○), 0.5 (▲), 1.0 (△), 2.0 (▼), 3.0 (▽), 4.0 (♦), 5.0 (◇), and 6.0 T (*).

In Fig. 5 we plotted the value of B^* and the zero field current density $j_s(B=0)$ at $T=4.2$ K versus the dislocation density for many films. We find that the characteristic field is directly proportional to the linear defect density as determined by wet chemical etching, $B^*\simeq0.7n_{disl}\Phi_0$ [Fig. 5(a)]. This implies that linear defects are the most important pinning centers in YBa$_2$Cu$_3$O$_{7-\delta}$ thin films, and that every linear defect pins one vortex.

Both $j_s(B=0)$ and B^* depend strongly on temperature. The current density $j_s(B=0)$ however does *not* depend systematically on the dislocation density [Fig. 5(b)]. The latter point is due to the fact, that at low magnetic fields, vortices are individually pinned and the pinning force depends only on the (single) vortex-pin potential. This point also shows that the self-field $\mu_0H_{self}\approx1/2j_sd$ (Refs. 64,65) (d is the thickness of the sample) does not influence the measurement of B^*. Although the self-field is of the same order of magnitude as the characteristic field, B^* is proportional to n_{disl} and does not depend on j_s or the sample dimensions like μ_0H_{self}. We conclude therefore that the plateau of $j_s(B)$ is not an experimental artifact connected to the self-field, but indeed related to the strong pinning of vortices by linear defects. In addition the field of first penetration, measured for
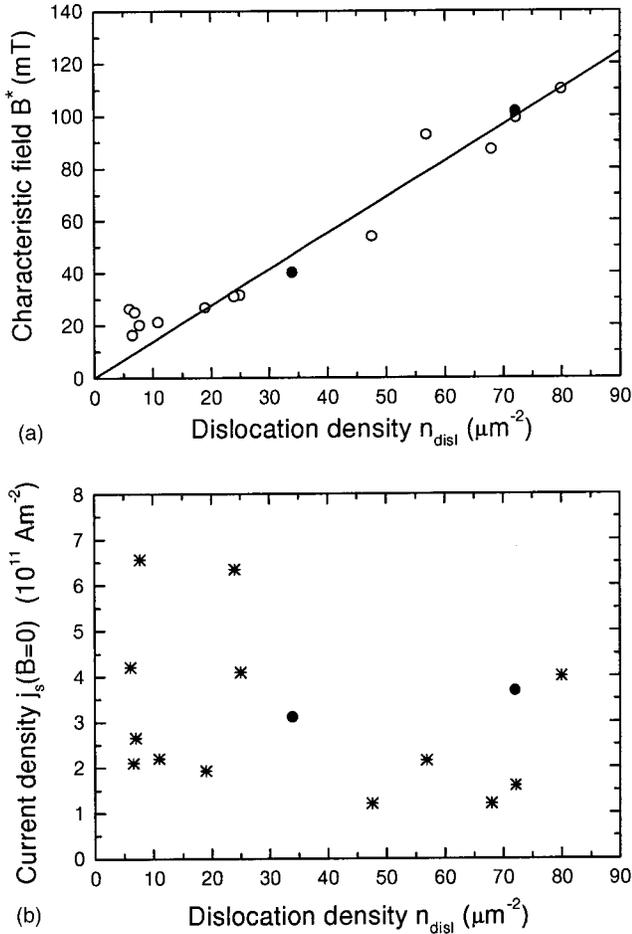
FIG. 6. Exponents $\alpha \equiv d \ln j_s / d \ln B$ at high magnetic fields for films: $E493$ (■), $F554$ (□), $D203$ (●), $C496$ (○) and $A67$ (▼). For films with a low dislocation density $\alpha \approx -0.58$, constant with temperature, whereas for films with many dislocations α is more negative and decreases with temperature. Note that the y axis is negative. Lines are guides to the eye.

FIG. 5. (a) Characteristic field B^* for various films at $T = 4.2$ K versus the dislocation density n_{disl}, showing that linear defects are the most important pinning source at low magnetic fields. (b) The superconducting current density $j_s(B=0)$ at $T = 4.2$ K is roughly constant for the many films we investigated, independent of the dislocation density. Solid circles denote the samples $C496$ and $E493$ from Figs. 3 and 4.

various samples both by torque magnetometery and magneto-optics $\mu_0 H_{pen} \approx 10-25$ mT$< B^*$.[49]

At higher magnetic fields we observe a transition to a power law behavior for films with a low dislocation density $j_s(B) \sim B^\alpha$, with $\alpha \approx -0.58$. This is close to $j_s(B) \sim 1/\sqrt{B}$. Typically such a field dependence is described by plastic pinning,[27] or a flux line shear model where the unpinned vortices are moving by shear forces through the lattice of strongly pinned vortices.[66] The power law behavior sets in at $\mu_0 H \cong 0.5$ T and extends to 7 T at low temperatures. At higher temperatures a faster decrease of $j_s(B)$ develops, that is accompanied by an exponential increase of the relaxation rate Q (see Fig. 9 and the next section). This does not necessarily mean that there is a crossover to another pinning mechanism. Merely the relaxation in this region becomes so strong that we cannot relate j_s to the true critical current density j_c even qualitatively. Therefore we cannot make any statements about the pinning mechanism without determining $j_c(B,T)$ by using, for example, the generalized inversion scheme.[67]
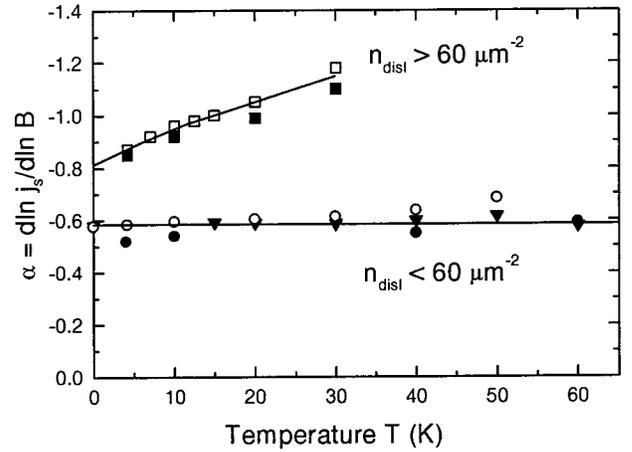
Eventually also in films with a large defect density a power law behavior is reached. However, as shown in Fig. 6, for films with high n_{disl}, $\alpha(T)$ decreases with temperature to $\alpha \approx -1.1$ at $T = 50$ K, whereas $\alpha(T) \approx -0.58$ constant for all T for the films with low n_{disl}. The crossover in behavior at high magnetic fields occurs when the dislocation density $n_{disl} \approx 60$ μm^{-2}. The reason for this crossover is possibly related to the distance between the linear defects in the film. For film $D203$ ($n_{disl} = 57$ μm^{-2}), the distance between defects is $d_r = 150$ nm$\cong \lambda$, whereas for $E493$ and $F554$, that have many dislocations, $d_r \approx 100$ nm$< \lambda$. Since $j_s \sim 1/B$ is the typical behavior for a collective pinning of the dislocation lattice, our result implies that the pinning mechanism changes from a shear ($\alpha = -1/2$) to a collective pinning regime ($\alpha = -1$) for $d_r < \lambda$. Note that also in irradiated single crystals (with $d_r \ll \lambda$) collective pinning with $j_s \sim 1/B$ is observed above B^*.[45] In Sec. V C we will address the high field behavior of j_s more thoroughly.

B. General properties of the dynamical relaxation rate Q

After describing the general properties of j_s, we turn to the dynamical relaxation rate. First we investigate the behavior of Q at low fields $\mu_0 H < B^*$, where j_s exhibits a plateau. To measure the relaxation Q at these fields, we have to use very low sweep rates to acquire sufficient data points. Moreover, the torque disappears at vanishing magnetic field. We use an external current source in combination with the magnet power supply to obtain sweep rates down to 90 μT s. In Fig. 7 the current density at four different sweep rates is plotted for film $D203$. As j_s exhibits a plateau at every sweep rate, so does the relaxation rate $Q(B)$ at fields below B^*. We thus observe in the relaxation the same matching effect as in j_s. The plateau in Q is also observed at higher temperatures (inset of Fig. 7) and like $B^*(T)$ the size of the plateau decreases with increasing temperature. If we increase
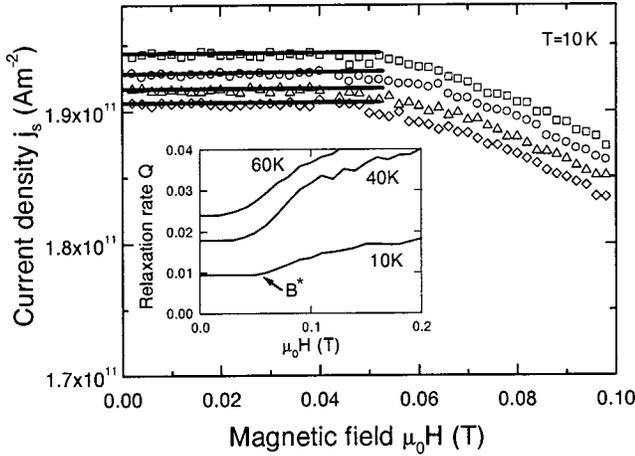
FIG. 7. Current density $j_s(B)$ at low magnetic fields for various sweep rates (film $D203$), $T=10$ K. $j_s(B)$ becomes constant at B^*, which is independent of the sweep rate used. From top to bottom: $dB/dt=735$, 368, 184, and 92 μT s. Inset: $Q(B)$ for $D203$ at $T=10$, 40, and 60 K. The decrease of B^* with temperature is clearly observed.

the magnetic field beyond the characteristic field B^*, $Q(B)$ increases steeply (see Fig. 8), especially at low temperatures. The relaxation rate rises until $\mu_0 H \approx 0.5$ T and becomes roughly constant for high magnetic fields at low temperatures.

The sharp increase of the relaxation just above B^* can be understood as a consequence of the crossover from strong pinning by dislocations towards another (weaker) pinning regime. It is comparable to the crossover observed in $j_s(B)$ from a plateau at low fields, to a power law decrease at high magnetic fields. When the current density decreases as a power law $j_s(B) \sim B^\alpha$, with $\alpha < 0$, $Q(B)$ is constant again. The behavior of $Q(B)$ is thus closely related to the behavior of $j_s(B)$.

There is an interesting difference in $Q(B,T)$ of films with low and high dislocation density; in films with a low dislo-
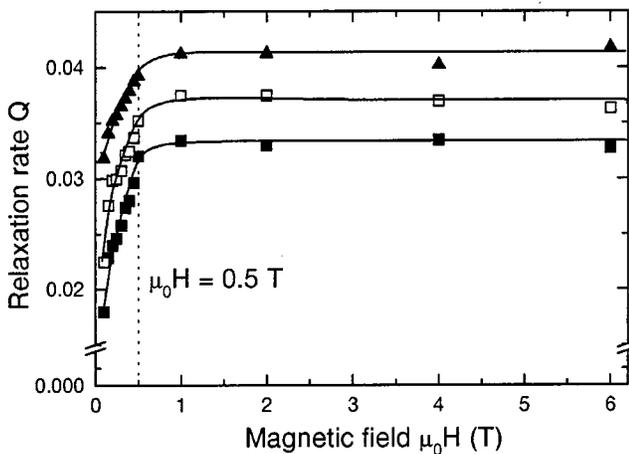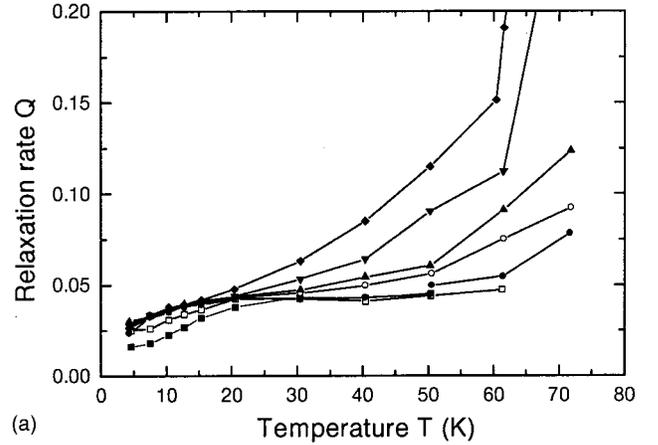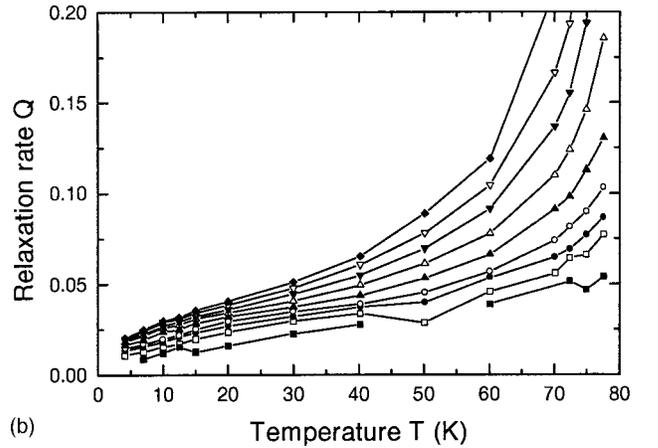

FIG. 8. $Q(B)$ at various low temperatures for film $A67$. At high magnetic fields, $Q(B)$ is constant, but when $\mu_0 H \lesssim 0.5$ T, the relaxation decreases sharply. From bottom to top $T=7(\blacksquare)$, 10 ($\square$), and 15 K ($\blacktriangle$). Lines are guides to the eye.

FIG. 9. Dynamical relaxation rate $Q(T)$ for (a) $A67$ and (b) $F554$. From bottom to top $B=0.1$ ($\blacksquare$), 0.3 ($\square$), 0.5 ($\bullet$), 1.0 ($\circ$), 2.0 ($\blacktriangle$), 3.0 ($\triangle$, only $F554$), 4.0 ($\blacktriangledown$), 5.0 ($\triangledown$, only $F554$), and 6.0 T ($\blacklozenge$).

cation density $Q(T)$ is constant at intermediate temperatures $20 < T < 50$ K (Fig. 9). This plateau has been observed before and seems to be a common feature for $YBa_2Cu_3O_{7-\delta}$.[68] However, in films with high n_{disl}, Q increases monotonically with T.

At low temperatures $T \lesssim 10$ K a transition from thermally activated creep to quantum creep takes place and $Q(T)$ becomes independent of temperature.[69] Especially in Fig. 9(a) for the lowest field values, $B=0.1,0.3$ T, one distinguishes that $Q(T)$ starts to flatten. We do not discuss the effect of quantum creep, since it is described extensively elsewhere,[70] but for describing thermally activated flux motion, we have to discard data for $T \lesssim 10$ K.

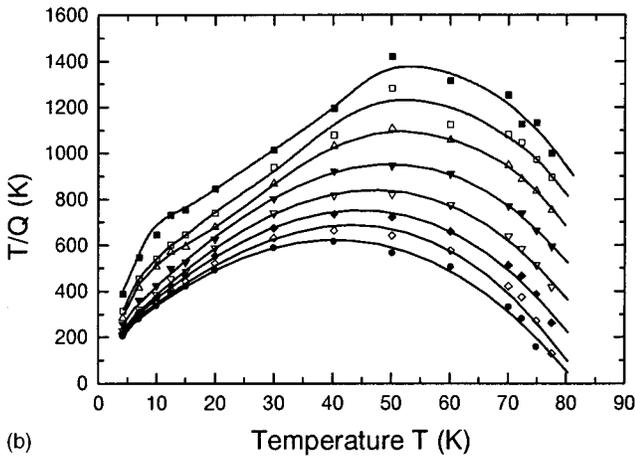### C. Determination of the pinning energy U_c

The pinning energy U_c can be determined directly from the dynamical relaxation rate. For thermally activated flux creep, the probability of a vortex jumping from one pinning configuration to another is $P \propto e^{-U(j,B,T)/k_B T}$. The activation energy is given by[71]

$$U(j) = \frac{U_c}{\mu}\left(\left(\frac{j_c}{j_s}\right)^\mu - 1\right) = Ck_B T, \tag{18}$$
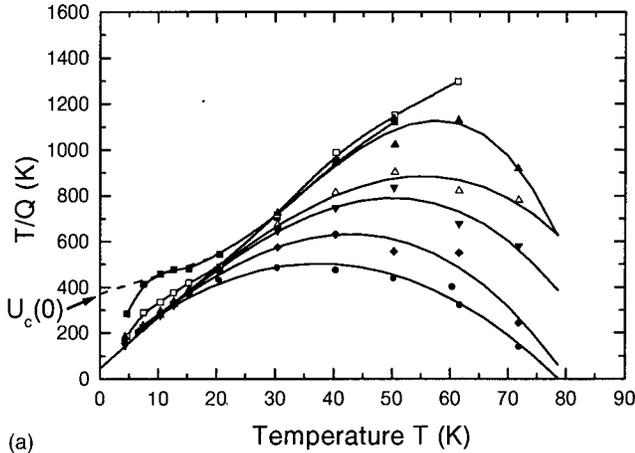
(a)

(b)

FIG. 10. T/Q vs T plots for two films (a) $A67$ and (b) $F554$ at $B=0.1$ (■, only $A67$), 0.3 (□), 0.5 (▲), 1.0 (△), 2.0 (▼), 3.0 (▽, only $F554$), 4.0 (◆), 5.0 (◇, only $F554$), and 6.0 T (●). Lines are guides to the eye. Extrapolation of T/Q to $T=0$ gives the pinning energy U_c. At high magnetic fields the pinning energy becomes independent of magnetic field. At low magnetic fields an upturn appears, that is specifically clear in $A67$, resulting in an increase of $U_c(B)$. At low temperatures $T \lesssim 10$ K the curves bend down to zero due to quantum creep.

where μ is a model dependent parameter, k_B the Boltzmann constant and C a factor that incorporates the attempt frequency of the vortex to jump over a potential barrier and the geometry of the sample. C depends logarithmically on the sweep rate dB/dt. After extracting j_s from Eq. (18) and differentiating to dB/dt one obtains the following relationship for U_c:

$$\frac{T}{Q} = \frac{U_c}{k_B} + \mu C T. \tag{19}$$

Equation (19) provides us with a direct measure of U_c, if we plot T/Q vs T and extrapolate to $T=0$. Note that we have to neglect the data below $T \lesssim 10$ K, because of quantum creep. Figure 10 shows a plot of T/Q of the films $A67$ and $F554$ ($n_{\text{disl}}=7$ and $n_{\text{disl}}=90$ μm^{-2}). Indeed at the lowest temperatures ($T=4.2$ and 7 K) T/Q bends down towards T
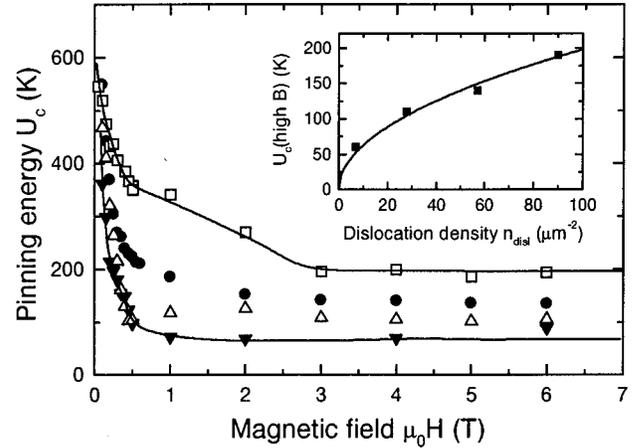

FIG. 11. Pinning energies U_c for various films: $A67$ (▼), $B670$ (△), $D203$ (●), and $F554$ (□). At high fields U_c exhibits a plateau, whereas at low magnetic fields, it rises steeply to $U_c(B=0) \approx 600$ K. Lines are guides to the eye for $A67$ and $F554$. Inset: plateau of U_c at high magnetic fields scales with the square root of the dislocation density $\sqrt{n_{\text{disl}}}$.

$=0$, which corresponds to a constant relaxation rate $Q(T)$ due to quantum creep. At intermediate temperatures the relaxation rate is more or less constant and T/Q rises linearly. At higher temperatures however, thermal fluctuations become stronger and Q increases exponentially, which results in a sharp decrease of T/Q. An interesting feature is observed in Fig. 10(a); at low magnetic fields $\mu_0 H \lesssim 0.5$ T, an upturn develops. This behavior is directly coupled to the decrease of the relaxation rate, being constant at high magnetic fields and exhibiting a sharp decrease for $\mu_0 H \lesssim 0.5$ T at low temperatures (Fig. 8). Especially in film $A67$ the upturn is very clear but, although less pronounced, it is also observed in other films. At high magnetic fields the lines of T/Q fall almost on top of each other [$Q(B)$ is virtually constant at high magnetic fields], indicating that the pinning energy U_c is only weakly field dependent.

In Fig. 11 we plotted the pinning energy versus the magnetic field. We can distinguish the same field regimes as for the relaxation. At low magnetic fields U_c extrapolates to a value of $U_c \approx 600$ K. At high magnetic fields $U_c(B)$ is roughly constant with $U_c \approx 60-200$ K. The plateau in $U_c(B)$ scales with the square root of the dislocation density (inset of Fig. 11), which shows that the dislocation lattice is still important at high magnetic fields, when the vortices outnumber the strong pinning centers by far. Note that a similar field dependence of $U_c(B)$ in YBa$_2$Cu$_3$O$_{7-\delta}$ films has been observed before by Douwes and Kes.[11]

One might be tempted to conclude that $U_c(B=0) =600$ K is the pinning energy of a single vortex, pinned by a linear defect. However, a simple calculation of the pinning energy U_p, obtained by equating U_p to the Lorentz force $j_s \Phi_0 d$ times the range of the pinning potential, yields $U_p \sim 10^4$ K, which is at least one order of magnitude higher than observed experimentally. The discrepancy between the experimental and theoretical pinning energies seems at first sight paradoxal, but one should realize that U_c is related to Q

and thus to the elementary excitations of a vortex. The critical current density on the other hand is related to the depinning of a complete vortex from its defect and therefore to the condensation energy ε_0 that is much larger. In Sec. V E we will investigate what kind of excitation is responsible for the observed pinning energy U_c.

V. DISCUSSION

A. Current density at low magnetic fields

At low temperatures and for large defects, j_c is comparable to the depairing current; see Eq. (4). In thin films and in irradiated crystals the current density is typically reduced compared to the depairing current j_0, because the linear defect size in films nor the typical radius of columnar tracks are in the limit of $x \gg 1$. We incorporate all current reducing effects into one parameter $\eta \equiv j_c/j_0$, denoting the pinning efficiency, as was done for irradiated single crystals by Civale et al.[16] Experimentally we find, with $j_c \approx 5 \times 10^{11}$ A m^{-2} and $j_0 \approx 4 \times 10^{12}$ A m^{-2}, that $\eta = 0.13$, which is comparable to the values obtained for columnar tracks, $\eta = 0.17$.[45] The maximum pinning efficiency can be obtained from Eq. (10), and gives $\eta \approx 0.22$ for thin films [taking $r_r \approx 2\xi(0)$], and $\eta \approx 0.32$ for irradiated crystals [taking $r_r \approx 4\xi(0)$]. These maximum pinning efficiencies are close to the experimental values, which shows that the superconducting order parameter is almost completely suppressed inside the defect.

In irradiated thin films an increase of the critical current density was observed compared to unirradiated thin films. The increase ranges typically from a few tens of percents[28] to a factor 2,[29,33] which can be directly explained by the larger size of the columnar tracks compared to natural linear defects. From Eq. (10) we find that for $r_r \approx \xi(0)$ the critical current density is roughly proportional to r_r. An increase of j_c by a factor 2 would imply that the columnar defects are about twice as large as natural linear defects, which is indeed the case. Schuster et al.[30] found that the relative increase of j_c in thin YBa$_2$Cu$_3$O$_{7-\delta}$ films before and after irradiation depends on the type of ion used. Heavy-ion irradiation by Pb ions was most effective and showed an increase of j_c by a factor 5. This difference cannot be fully explained by the larger size of columnar defects, but the differences between intrinsic current densities measured in various films can be significant [see Fig. 5(b)]. Moreover the maximum current, measured by Schuster et al.[30] in a Pb-irradiated film, $j_c = 6.7 \times 10^{11}$ A m^{-2} is about 30% larger than in our film $F554$. This implies that $r_r \approx 4$ nm for Pb-irradiated columnar defects, which is quite a reasonable estimate.

Other reports on irradiated thin films focus on the angular dependence of the pinning force, showing a peak in the irradiation direction,[72,73] or investigating Bose glass scaling in irradiated thin films.[74,75] Unfortunately irradiation doses and, consequently, the magnetic fields considered, are usually much larger than the typical matching fields of natural linear defects ($B_\Phi \approx 100$ mT), which makes comparison to our films difficult. To observe Bose glass scaling by natural linear defects, one would have to measure at very low fields. Note that Roas et al.[76] did observe a peak in the critical

current density along the c axis in as-grown YBa$_2$Cu$_3$O$_{7-\delta}$ thin films, that could well be caused by linear defects.

To compare the measured superconducting current density $j_s(T)$ with the true critical current density $j_c(T)$, whose temperature dependence was derived by theory, we need to compensate for relaxation effects. The relation between $j_s(B=0,T)$ and $j_c(B=0,T)$, derived from Eqs. (18) and (19) is

$$\frac{j_s}{j_c} = (1 - \mu C Q)^{1/\mu}. \tag{20}$$

From plots of T/Q vs T in Fig. 10 we find the product μC at low magnetic fields. Independently we determine the activation constant $C \approx 15-19$,[77] which results in $\mu \approx 1$. The ratio j_s/j_c is only weakly temperature dependent at intermediate temperatures 10 K $< T <$ 50 K. This is not surprising, because $Q(T)$ is roughly constant at intermediate temperatures [see Fig. 9(a) and Ref. 68]. Furthermore j_s/j_c does not depend sensitively on μ, which enables us to treat pinning models for the critical current density at $B=0$, provided that we correct the measured current density j_s using Eq. (20).

In Fig. 12 the measured $j_s(T)$ is plotted for films $A67$ and $F554$, together with $j_c(T)$, corrected according to Eq. (20) with $\mu = 1$ and $C = 15$ for $A67$, and $C = 19$ for $F554$. Also included is the expected temperature dependence according to $j_c(T) \sim 1/(\lambda^2(T)\xi^\nu(T))$, with $\nu = 1$, 2 and $\nu = 3$. For the temperature dependences we have taken $\lambda(T) = \lambda(0)(1-t^4)^{-1/2}$ and $\xi(T) = \xi(0)[(1+t^2)/(1-t^2)]^{1/2}$, with $t = T/T_c$.

We find good agreement with the measured current densities with $\nu = 3$ for $A67$ and $\nu \approx 2$ for $F554$. Secondly we find that thermal fluctuations have a small effect on $j_c(T)$, which was expected, since $\tilde{T}^r_{dp} \approx 400$ K $\gg T$. From the values obtained for ν we conclude that the linear defects in $A67$ are smaller in average than those in film $F554$. Indeed from AFM measurements we found, that the sputtered film $A67$ contains twice as much edge dislocations as screw dislocations, whereas in the laser ablated films, like $F554$, only screw dislocations were found. Since the Burgers vector of screw dislocations is directed along the c axis, it is 3 times larger than that for edge dislocations. We therefore expect that the defect core size, typically a few Burgers vectors, is larger in film $F554$. TEM observations from Gao et al.[78] indicated that $r_r \approx 1.0$ nm $\approx 2.5|b|$ for an edge dislocation in a YBa$_2$Cu$_3$O$_{7-\delta}$ thin film. For screw dislocations we then expect $r_r \approx 3.0$ nm $\approx 2\xi(0)$. A rough estimate for the average defect size in film $A67$ yields $\bar{r}_r \approx 1.3$ nm $\approx 0.9\xi(0)$, whereas in film $F554$ we would get $r_r \approx 3.0$ nm $\approx 2\xi(0)$.

Filling in $r_r = 0.9\xi(0)$ and $r_r = 2\xi(0)$ in the general equation for $j_c(T)$, given by Eq. (10), and determining ν by fitting with $j_c(T) \sim 1/(\lambda^2(T)\xi^\nu(T))$, we find $\nu = 2.0$ and $\nu = 2.8$, respectively, which is in excellent agreement with the values from Fig. 12. Moreover, if we calculate $j_c(0)$ from $f_{max} \approx -d\varepsilon_r/dR|_{R=r_r}$ we find $j_c(0) \approx 2.0 \times 10^{11}$ A m^{-2} for film $A67$ and $j_c(0) \approx 5.1 \times 10^{11}$ A m^{-2} for film $F554$, again in good agreement with experiment.

Comparing the current density below the characteristic magnetic field for various films, we find that $j_s(B=0)$ is
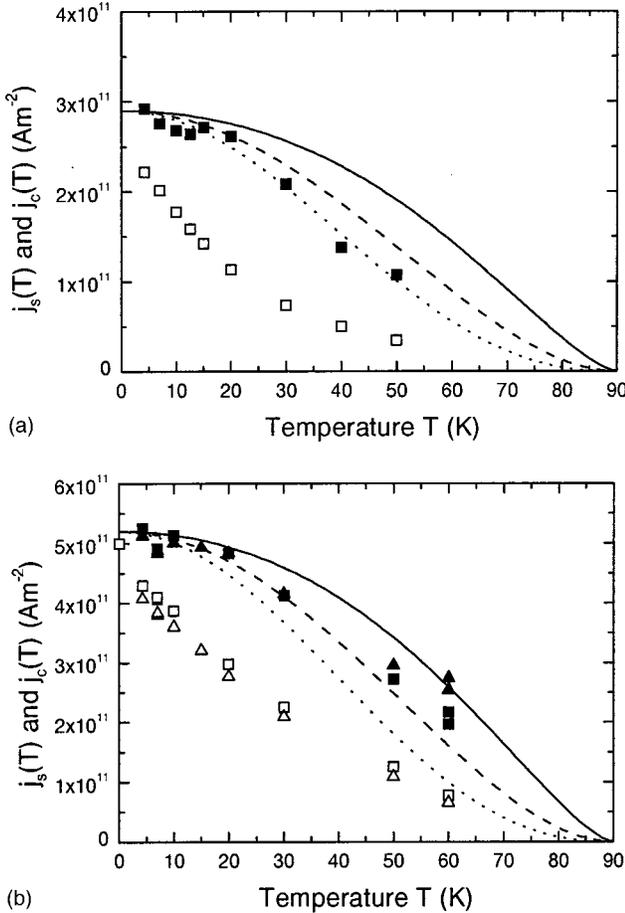
(a)

(b)

FIG. 12. Temperature dependence of the current densities j_s (open symbols) and j_c (solid symbols) for films $A67$ (a), $B = 0.1$ T ($\square,\blacksquare$), and $F554$ (b), $B = 0.1$ T ($\square,\blacksquare$) and $B = 0.2$ T ($\triangle,\blacktriangle$). Lines depict the derived dependence $j_c(T) \sim 1/\lambda^2(T)\xi^\nu(T)$ with $\nu = 1$ (solid lines), $\nu = 2$ (dashed lines), and $\nu = 3$ (dotted lines). From the fits it is obvious that the average linear defect size of film $A67$ is smaller than that of film $F554$.

essentially independent of the dislocation density. Some films with higher dislocation density $n_{\text{disl}} \gtrsim 50 \ \mu\text{m}^{-2}$, show a somewhat reduced current density at $T = 4.2$ K. We believe that this is due to the slightly reduced crystallinity for films with large n_{disl} (smaller T_c, wider rocking curve $\Delta\omega_{(005)}$), so that the intrinsic current density is smaller in films with large n_{disl}. However, also the defect sizes may vary somewhat from film to film (like in $A67$ and $F554$). The fact that $j_s(B=0)$ is independent of the dislocation density implies that surface roughness pinning in films is, at least at low magnetic fields, not important, contrary to what has been claimed by some groups.[7,8] Because the island density (and thus the surface roughness) increases with increasing dislocation density, surface roughness pinning would give a higher current density for high dislocation density films. This is not observed; in fact from all our measurements, we see that the current density is typically somewhat lower for films with many dislocations, compared to films with a low dislocation density [see Fig. 5(b)].
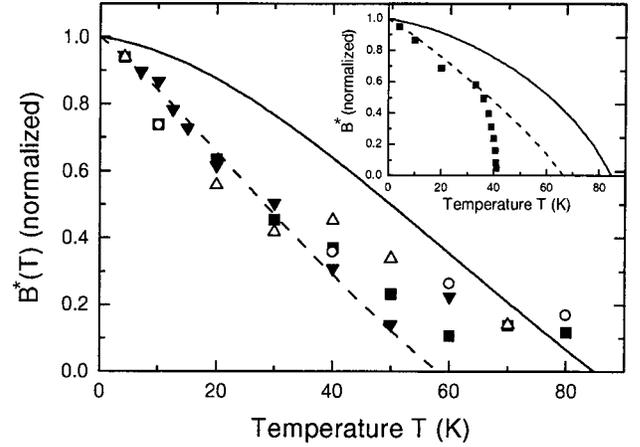

FIG. 13. Normalized temperature dependence of the characteristic field $B^*(T)$ for films $B670$ ($\triangle$), $A67$ ($\blacktriangledown$), $D203$ ($\bullet$), and $E493$ ($\blacksquare$). Lines are the expected temperature dependence with $\tilde{T}^r_{dp}(0) = 400$ K (solid line), and $\tilde{T}^r_{dp}(0) = 70$ K (dashed line). At higher temperatures $T \gtrsim 30$ K, deviations occur because the harmonic oscillator potential only valid when $T \ll \tilde{T}^r_{dp}(T)$. Inset: Normalized characteristic field $B^*(T)$ of an irradiated crystal (from Ref. 45), together with the expected temperature dependence with $\tilde{T}^r_{dp}(0) = 400$ K (solid line) and $\tilde{T}^r_{dp}(0) = 95$ K (dashed line). Note that $\tilde{T}^r_{dp}(T) \sim 1/\lambda^2(T)$.

B. Characteristic field

The characteristic field B^* in thin films and in irradiated single crystals has the same physical origin, but in thin films B^* marks the end of a plateau in $j_s(B)$, whereas in single crystals the current density depends strongly on magnetic field, even below the matching field. The reason for this difference is the strong influence of vortex-vortex interactions in irradiated crystals, due to the high density and the random distribution of the columnar defects. The characteristic field in single crystals coincides with the matching field B_Φ, except for very high irradiation doses.[45] For YBa$_2$Cu$_3$O$_{7-\delta}$ films $B^* < B_\Phi$ and from the proportionality factor $B^*/B_\Phi = 0.7$ and Eq. (1) we estimate $\varepsilon_r/\varepsilon_0 \approx 0.18$.

The temperature dependence of $B^*(T)$, plotted normalized to its zero temperature value in Fig. 13, shows a similar dependence in films with low and high dislocation density. At low temperatures the reduction in B^* corresponds to the behavior found in irradiated YBa$_2$Cu$_3$O$_{7-\delta}$ crystals (see the inset of Fig. 13 and Ref. 34), but the sudden decrease of the matching field in irradiated crystals at around $T = 40$ K is absent in thin films.

To explain the decrease of $B^*(T)$ with increasing temperature we have to determine the temperature dependence of $\varepsilon_r/\varepsilon_0$, including the effect of thermal fluctuations, that facilitate the depinning of a vortex from its pinning site:

$$B^*(T) = B^*(0)\left(1 - \frac{T}{\tilde{T}^r_{dp}(T)}\right)\ln\left(1 + \frac{r_r^2}{2\xi(T)^2}\right). \quad (21)$$

If we use $\tilde{T}^r_{dp}(T) = \tilde{T}^r_{dp}(0)(\lambda^2(0)/\lambda^2(T))$, with $\tilde{T}^r_{dp}(0) = 400$ K (solid lines in Fig. 13), there is no agreement with
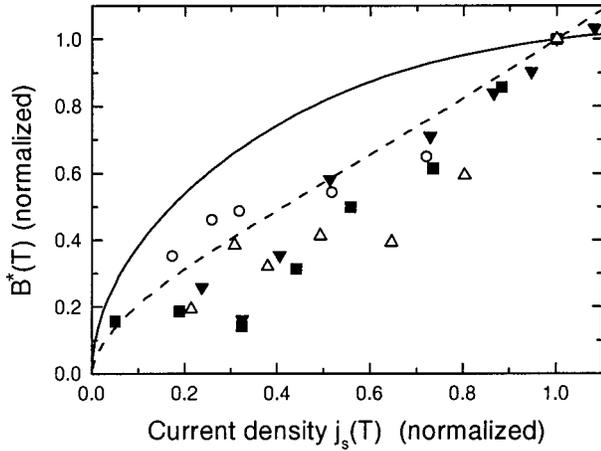
FIG. 14. Characteristic field $B^*(T)$, plotted versus $j_s(T)$ for films $B670$ ($\triangle$), $A67$ ($\blacktriangledown$), $C496$ ($\circ$), and $E493$ ($\blacksquare$). Both $B^*(T)$ and $j_s(T)$ are normalized to $T=10$ K. Lines are expected dependencies with $j_s(T)=j_c(T)[1-CQ(T)]$ and $B^*(T)\sim\ln(1+x^2(T))f(T/\tilde{T}^r_{dp})$ [Eq. (21), solid line] and $B^*(T)\sim\ln(1+x^2(T))f(T/\tilde{T}^r_{dp})[1-CQ(T)]$ (thermal activation included, dashed line).

the experimental data. Both in irradiated crystals and in thin films (Fig. 13) the measured $B^*(T)$ decreases faster than theory predicts, which was noted already by Thompson et al. for the case of irradiated crystals.[79] To explain the fast decrease of $B^*(T)$ one can of course assume a lower depinning energy. For example taking $\tilde{T}^r_{dp}(0)=70$ K for thin films (dashed line in Fig. 13) and $\tilde{T}^r_{dp}(0)=95$ K for irradiated crystals (dashed line in the inset of Fig. 13) gives a good agreement with the experimental data at low temperatures. But taking a different depinning energy changes the temperature dependence of $j_c(T)$ as well, and we cannot obtain a consistent picture for both $j_c(T)$ and $B^*(T)$ with a single $\tilde{T}^r_{dp}(0)$.

To illustrate this inconsistency more clearly we have plotted in Fig. 14 the temperature dependence of $B^*(T)$ versus the superconducting current density $j_s(T)$ for various films. The solid line is the expected curve, from Eq. (21) and $j_s(T)=j_c(T)[1-CQ]$ [taking $\tilde{T}^r_{dp}(0)=400$ K, $C=19$, $\nu=2$, and $Q(T)$ from experiment], which clearly does not describe the behavior observed in experiment. Note, that this does not depend on choosing $\tilde{T}^r_{dp}(0)$, since both $B^*(T)$ and $j_s(T)$ contain the same factor $f(T/\tilde{T}^r_{dp})$.

However, we have to realize that the size and temperature dependence of $B^*(T)$ were derived for $j_s=0$, whereas in our experimental situation large currents run through the film. As the pinning landscape tilts when applying a current, vortices escape more easily from the linear defect, and thus the characteristic field decreases. If we include the same factor $j_s/j_c=1-CQ(T)$ in the temperature dependence of $B^*(T)$, we obtain a good approximation of B^* (dashed line in Fig. 14). Apparently an increased relaxation rate results in a decrease of $B^*(T)$. Intuitively this is logical, but up to now there is no model available to describe this effect. A similar effect is observed in irradiated crystals, where the sudden

decrease of $B^*(T)$ at $T=40$ K (Ref. 45, and the inset of Fig. 13), is accompanied by a sharp increase of the relaxation rate $S(T)$, resulting in a peak in $S(T)$.[45,79]

C. Current density at high magnetic fields $\mu_0 H \gg B^*$

Whereas the pinning below the characteristic field is quite well understood, the situation at higher magnetic fields $\mu_0 H \gg B^*$ is less clear. Several models have been proposed. Douwes et al.[6] suggested, that at high magnetic fields, pinning is caused oxygen vacancies in the CuO_2 plane. Another possibility, suggested by Wördenweber,[66] is that at high magnetic fields there is a strongly pinned vortex lattice in the linear defects, whereas the unpinned vortices move by shearing in channels through the pinned lattice. A similar shear model, giving rise to plastic pinning is described by the Bose glass theory.[27] At high magnetic fields individually pinned vortices experience a transition to bundle pinning. The large density of vortices and the variety of pinning defects and models make it hard to interpret unambiguously the experimental data. Up to now no consistent picture for pinning at high magnetic fields has emerged.

Experimentally the most remarkable feature of the high field behavior of $j_s(B)$ is the change of slope $\alpha \equiv d\ln j_s/d\ln B$ from $\alpha=-0.58$ to $\alpha=-0.8$ to -1.1. This abrupt change of slope, observed when $n_{disl}>60$ μm^{-2} (which means that the average defect spacing $d_r<\lambda$), marks the onset of strong vortex interactions. The Bose glass theory,[27] that distinguishes between plastic pinning and collective pinning, provides a useful framework to describe our observations.

In plastic pinning the vortices, not accommodated by the dislocations, are pinned via shear interactions with the strongly pinned vortex lattice. The maximum pinning force is given by $f_{p,max}=c_{66}a_0$, where c_{66} is the shear elastic constant and a_0 the intervortex distance. The critical current density

$$j_c(B) \approx \eta \frac{\sqrt{\Phi_0}}{16\pi\mu_0\lambda^2_{ab}} \frac{B_\Phi}{\sqrt{B}} \approx \eta j_0 \frac{\xi}{\sqrt{\Phi_0}} \frac{B_\Phi}{\sqrt{B}} \qquad (22)$$

gives a field dependence of the current $j_c\sim B^{-0.5}$. The collective pinning model relates the Lorentz force within a correlation area of size $\sim R_c^2$ to the elastic force of the vortices. Collective pinning becomes important when the correlation radius $R_c\simeq d_r(\varepsilon_0/\varepsilon_r)(b_0/a_0)\simeq d_r$, the average defect spacing. The critical current density in this case is given by

$$j_c(B) \approx \eta \frac{\Phi_0}{4\pi\mu_0\lambda^2_{ab}\xi_{ab}} \frac{B_\Phi}{B} \approx \eta j_0 \frac{B_\Phi}{B}. \qquad (23)$$

The most important difference between Eqs. (22) and (23) is the field dependence that changes from $j_c\sim 1/\sqrt{B}$ to $j_c\sim 1/B$. Exactly such a crossover we observe experimentally when the average defect spacing becomes smaller than λ. We propose that collective pinning is important when $d_r<\lambda$, whereas in a more dilute linear defect lattice vortices are

plastically pinned. In irradiated single crystals, where $d_r \ll \lambda$, we expect collective pinning as well, which is indeed observed.[16]

There are, however, still a number unresolved questions. First the plastic pinning model gives too low estimates for the critical current density. For example, Eq. (22) with $B_\Phi = 0.1$ T and $B = 1$ T gives $j_c \approx 1 \times 10^9$ A m^{-2}. This is much lower than the measured value of typically $j_s \approx (1-2) \times 10^{11}$ A m^{-2} at $T = 4.2$ K and $B = 1$ T. This also implies that the low field current density, Eq. (10), and the high field current density, Eq. (22), do not connect at the matching field B_Φ [contrary to the collective pinning case, with Eqs. (10) and (23), note that $\eta \equiv j_c(0)/j_0$]. Matching the linear defect pinning and plastic pinning regimes would imply a dramatic decrease of $j_s(B)$ over two orders of magnitude between B^* and B_Φ. Instead we observe a smooth crossover to a power law regime, with only a minor decrease of $j_s(B)$. On the other hand, the plateau in U_c at high magnetic fields increases with the dislocation density (inset of Fig. 11), which can be perfectly understood in a plastic pinning model, since shearing through a defect lattice, filled with strongly pinned vortices, will be more difficult when the defect lattice is denser. Therefore a plastic pinning model is still a good candidate since it gives the right field dependence $j_s \sim 1/\sqrt{B}$ and explains why U_c increases with increasing dislocation density.

Secondly the slopes α do not coincide exactly with the theoretical dependencies. For films with high dislocation density $\alpha \approx -0.8$ at low temperatures, which is too low for collective pinning. Moreover, $|\alpha(T)|$ increases with temperature for films with high n_{disl}. Possibly the current density is determined by a mix of collective and shear pinning. After all we are still in a relatively low field regime, where $R_c \ll d_r$, and it is surprising that collective pinning occurs at all.

All discrepancies between theory and experiment point out that vortex-vortex interactions have a more profound influence on the current density than anticipated. One essential point, not considered up to now, is the nonrandom distribution of the linear defects in thin YBa$_2$Cu$_3$O$_{7-\delta}$ films. Due to the ordered distribution of the strongly pinned vortices at B^*, they provide a natural way for additional vortices to distribute themselves regularly, which improves the pinning properties at higher fields as well. In order to fully explain the measured size of j_s and its field dependence into more detail, these effects have to be taken into account more explicitly.

The temperature dependence of $\alpha(T)$ can be explained to a certain extent by the influence of the relaxation rate Q. Due to relaxation $\alpha \equiv d \ln j_s / d \ln B \neq d \ln j_c / d \ln B$. We can give a rough quantitative argument why the slopes of the power law behavior do not coincide exactly with the expected slopes in Eqs. (22) and (23). If we differentiate the general formula of thermally activated vortex creep, given by Eq. (18), with respect to the magnetic field B, we obtain the following expression:[80]

$$\frac{d \ln j_c}{d \ln B} = \frac{d \ln j_s}{d \ln B} + Q - CQ \frac{d \ln U_c}{d \ln B} = \alpha + Q - CQ \frac{d \ln U_c}{d \ln B}.$$

(24)

Thus, to obtain the field dependence of the true critical current density $d \ln j_c / d \ln B$, we have to add to the slope α two positive terms (note that in general $d \ln U_c / d \ln B \leq 0$). So the measured slope α is always more negative than the field dependence of the true critical current density. Comparing this with the measured slopes (Fig. 6), we observe that for films with low n_{disl}, $\alpha = -0.58$. This suggests that $j_c(B) \sim 1/\sqrt{B}$, with a correction of 0.08. Because α is constant with temperature, so should $Q(T)$ for these films. From Fig. 9(a) we learn that this is the case for films with a low dislocation density. For films with high n_{disl}, $\alpha \approx -0.8$ at low temperatures. With increasing temperature the slope decreases, but $Q(T)$ increases [Fig. 9(b)], so the correction terms are higher at larger temperatures, suggesting that $d \ln j_c / d \ln B$ is roughly constant with temperature. However, in that case the slope $d \ln j_c / d \ln B > -1$, so collective pinning cannot be the only mechanism determining j_c at high magnetic fields. The slope $d \ln j_c / d \ln B = -0.7 \pm 0.1$ has been found in numerical simulations of the plastic deformations due to strong pinning,[81] which could explain the observed slopes $\alpha = -0.8$ with a small correction according to Eq. (24). However, an exact calculation of the field dependence of the critical current would require a more thorough derivation, that includes in Eq. (24) also the field dependence of μ, which cannot be determined accurately within experiment.

D. Dynamical relaxation rate

Various pinning regimes are clearly seen in the field dependence of the relaxation rate $Q(B)$. Below B^* the relaxation rate is constant. Then it increases and becomes constant again for magnetic fields $\mu_0 H \gtrsim 0.5$ T. The same regimes are observed in $j_s(B)$ (showing first a constant plateau and in the second regime a power law behavior), and also in the pinning energy $U_c(B)$. This suggests that there are at least two regimes, one below B^* with strongly pinned vortices on the linear defects, and one above $\mu_0 H \gtrsim 0.5$ T with plastically or collectively pinned vortices. In between these two regimes the relaxation rate increases steeply.

The reason why the crossover occurs at about 0.5 T is not clear at present. In any case it is observed in various films independently of the dislocation density. Also it has been observed by other groups,[10,11] and in quantum creep.[70] The change in behavior at around $\mu_0 H = 0.5$ T is thus more general for YBa$_2$Cu$_3$O$_{7-\delta}$ films, and may well be related to a stronger influence of vortex-vortex interactions. The intervortex distance at this field $a_0 \approx 63$ nm $\approx \frac{1}{2}\lambda$, so the vortex-vortex interactions become increasingly more important from this field.

The temperature dependence of the relaxation at low fields is different from the situation in irradiated single crystals. Whereas in thin films $Q(T)$ rises monotonically, in irradiated crystals the conventional relaxation rate $S(T)$ exhibits a peak for $\mu_0 H < B^*$.[45,79] This peak marks the crossover of a single vortex regime, where the motion of vortices takes place via variable range hopping, to a collective pinning regime involving vortex bundles.[79] In thin films a similar peak of $Q(T)$ is absent, because both variable range hopping and bundle pinning do not occur in thin films at $\mu_0 H \simeq B^*$. A

necessary condition for variable range hopping is a strong dispersion in the pinning energies and/or the distances between the strong pinning sites.[39] In single crystals irradiation indeed produces randomly distributed columnar tracks of various strength, but in thin films the dispersion in pinning energies of the dislocations is much smaller, as is the variation in distances between the defects.[44] Secondly, vortex bundles are not formed in thin films just above the characteristic field $\mu_0 H \gtrsim B^*$, because the field value $B^* \lesssim 100$ mT is too small. In thin films B^* marks a different crossover in vortex pinning, namely dislocation pinning governed by half-loop excitations (see Sec. V E) towards a plastic or collective pinning regime that sets in at higher magnetic fields (Sec. V C).

The absence of a peak in the relaxation rate is clear from $j_s(T)$ as well, because $Q(T)$ is directly related to the behavior $d \ln j_s / dT$. In irradiated crystals $d \ln j_s / dT$ shows a minimum when $\mu_0 H < B^*$, but this minimum is absent in thin films. This illustrates once more the close relationship between the relaxation rate $Q(T)$, or equivalently $S(T)$, and the derivative of the current density $d \ln j_s / d \ln T$, as was found in the magnetic field dependence of the relaxation $Q(B)$, Eq. (24). In fact an expression similar to Eq. (24) was derived in Ref. 45, relating the temperature dependence j_s to the relaxation rate $S(T)$.

E. Pinning energy U_c

According to the Bose-glass theory the vortex excitations that determine the pinning energy U_c at high driving currents are half-loop excitations. For half-loop excitations the activation energy is calculated by balancing the driving force with the loss in pinning energy and the increase of elastic energy. It is given by[42]

$$U(j) = \xi \sqrt{\varepsilon_l \varepsilon_r(T)} \left(\frac{j_c}{j_s} - 1 \right) = U_c(T) \left(\frac{j_c}{j_s} - 1 \right), \quad (25)$$

with ε_r the depth of the pinning potential and ε_l the line tension, which is smaller than ε_0 due to anisotropy. Note that $\tilde{T}_{dp}^r \equiv b_0 \sqrt{\varepsilon_l \varepsilon_r}$, which means that the depinning energy and half-loop energy are comparable in size. With $\xi = 1.5$ nm and $\varepsilon_l \approx \varepsilon_r \approx 0.2 \varepsilon_0$ we estimate that $U_c(0) \approx 250$ K, which is smaller than the experimentally obtained value $U_c(0) \approx 600$ K, but given the uncertainty in the parameters used, the estimate is not so bad.

The temperature dependence of $U_c(T)$ is given by

$$U_c(T) = U_c(0) \frac{\lambda^2(0) \xi(T)}{\lambda^2(T) \xi(0)} \sqrt{f(T/\tilde{T}_{dp}^r)} \approx \frac{\xi(T)}{\lambda^2(T)} \sqrt{f(T/\tilde{T}_{dp}^r)}. \quad (26)$$

To check whether or not this kind of excitation is consistent with experiment, we can use the temperature dependence of $U_c(T)$ to calculate the ratio j_s / j_c. Half-loop excitations impose that the glass exponent in Eq. (18) $\mu = 1$, which implies that

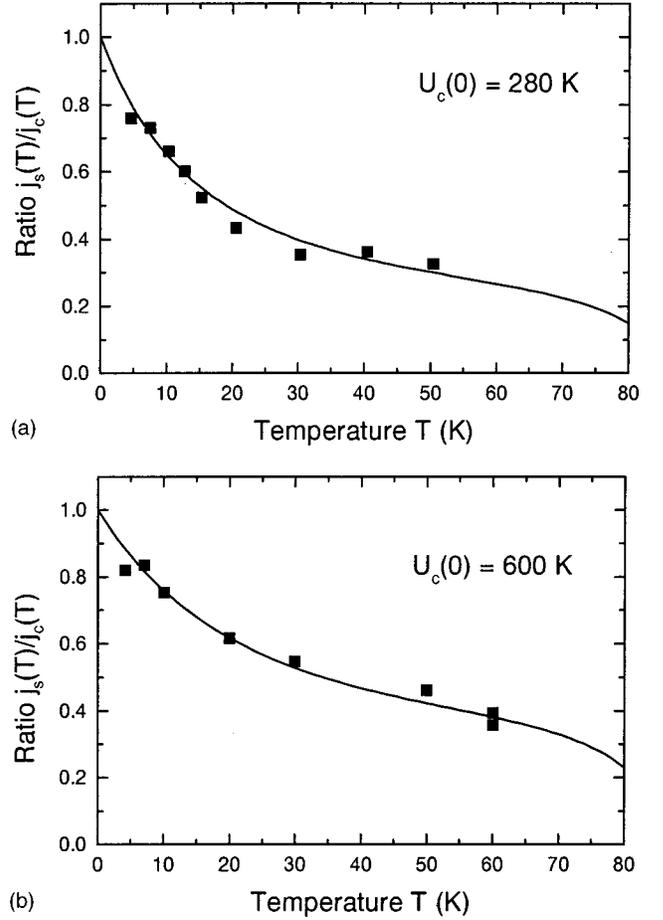$$\frac{j_s(T)}{j_c(T)} = \frac{1}{1 + C k_B T / U_c(T)}. \quad (27)$$

FIG. 15. Ratio j_s / j_c from experiment and theory for films (a) $A67$ and (b) $F554$. Solid squares are obtained from experiment. Solid lines correspond to the theoretical behavior for half-loop excitations Eqs. (26) and (27), with $\mu = 1$, $C = 15$ ($A67$), or $C = 19$ ($F554$), $\tilde{T}_{dp}^r(0) = 400$ K, and $U_c = 280$ K for $A67$ and $U_c = 600$ K for $F554$.

In Fig. 15 we plotted the ratio $j_s / j_c = 1 - CQ$ from experiment together with the expected temperature dependence, given by Eq. (27). We took $\tilde{T}_{dp}^r(0) = 400$ K, and the usual temperature dependence for $\lambda(T)$ and $\xi(T)$. We find excellent agreement with experiment, if we take for $U_c(0) = 280$ K for $A67$ and $U_c(0) = 600$ K for $F554$. This agrees with the pinning energy, measured experimentally at $B = 0.1$ T, $U_c = 360$ K and $U_c = 520$ K for film $A67$ and film $F554$, respectively. Note, that $B = 0.1$ T is larger than B^* for film $A67$. Therefore $U_c = 360$ K < 600 K, since the pinning energy decreases steeply beyond B^*. Unfortunately no relaxation data was available at lower magnetic fields.

An important question is whether the assumption, that the glass exponent $\mu = 1$, is correct at low fields. From the low temperature slope of the plots T/Q vs T, Fig. 10, we find $\mu \approx 1 - 1.3$ at high magnetic fields $\mu_0 H > 0.5$ T, but for low fields μ is decreasing towards $\mu \approx 0.5$ at $\mu_0 H = 0.1$ T. The order of magnitude of μ is reasonable, but its field dependence is puzzling. For variable range hopping, theory predicts μ to increase from 1/3 to 1 with increasing magnetic field,[27,42] which is similar to the increase of $\mu(B)$ we ob-

serve in experiment. Assuming a somewhat higher C we find even quantitative agreement with the theory for variable range hopping. But, as we argued in the previous section, variable range hopping is unlikely to occur in our films, due to the large distances between defects. It involves a pinning energy of typically $U_c \simeq d_r \sqrt{\varepsilon_l \varepsilon_r}$, which is at least one order of magnitude larger than the energy required for half-loop excitations. On the other hand, in film $A67$, that contains both edge and screw dislocations we have a larger dispersion in the pinning potential ε_r, which facilitates variable range hopping. Indeed in the T/Q vs T plot [Fig. 10(a)] the decrease of $\mu(B)$ with magnetic field is more apparent than in film $F554$.

The length l_{hl} of the half-loop and the displacement u_{hl} of a half-loop excitation[39] are of the order of a few nanometer, in agreement with other estimates for the activation length. Hylton and Beasley[1] obtained earlier similar values for the length of a vortex segment, being depinned from a linear row of point pins. Also at very low temperatures, Hoekstra *et al.*[82] found that the correlation length L_c is of the order of a few nanometers. We conclude that half-loops provide the most likely mechanism for vortex excitations at low magnetic fields, but the measured values of the glass exponent remain unexplained by theory. In any case the ratio j_s/j_c from experiment is consistent with a pinning energy $U_c(T)$ of half-loop excitations, and moreover it has the correct temperature dependence.

At high magnetic fields the pinning energy is essentially constant. Its magnitude appears to be proportional to the square root of the dislocation density [inset of Fig. 11]. We propose that pinning of vortices in the high field regime is caused by the collective pinning of vortex bundles, between the array of strongly pinned vortices. Assuming that it involves plastic pinning of vortex bundles of volume V_c we have[42]

$$U_c(B) \simeq \sqrt{c_{44}\bar{E}_{\text{pin}}}V_c \simeq \sqrt{c_{44}c_{66}(a_0/d_r)^2}V_c$$

$$\simeq \frac{\Phi_0 \sqrt{B}}{16\pi\mu_0\lambda^2}\sqrt{B_\Phi}V_c, \qquad (28)$$

which gives the observed dependence of $U_c(B) \propto \sqrt{B_\Phi}$ $\propto \sqrt{n_{\text{disl}}}$. The field dependence of $U_c(B)$ implies that $V_c(B)$ $\sim 1/\sqrt{B}$. The collective pinning volume according to Eq. (28) and the inset of Fig. 11 at $\mu_0 H = 0.5$ T is V_c $\approx 5.3 \times 10^{-24}$ m^3. Taking the intervortex distance at $\mu_0 H$ $= 0.5$ T for the collective pinning radius, i.e., $R_c = 63$ nm, we obtain $L_c \approx 1.3$ nm. A theoretical estimate for R_c $\simeq d_r(\varepsilon_0/\varepsilon_r)(b_0/a_0) \approx 24$ nm gives $L_c \approx 9.3$ nm. These values of typically a few c-axis lattice distances agree well with other estimates (see, for example, Doyle *et al.*, Ref. 83) for the collective pinning length and for the size of the half-loop excitations along the c axis.

VI. CONCLUSIONS

Natural linear defects have a profound effect on the pinning properties of high-T_c YBa$_2$Cu$_3$O$_{7-\delta}$ thin films. We have shown that indeed many features, both in the field and tem-
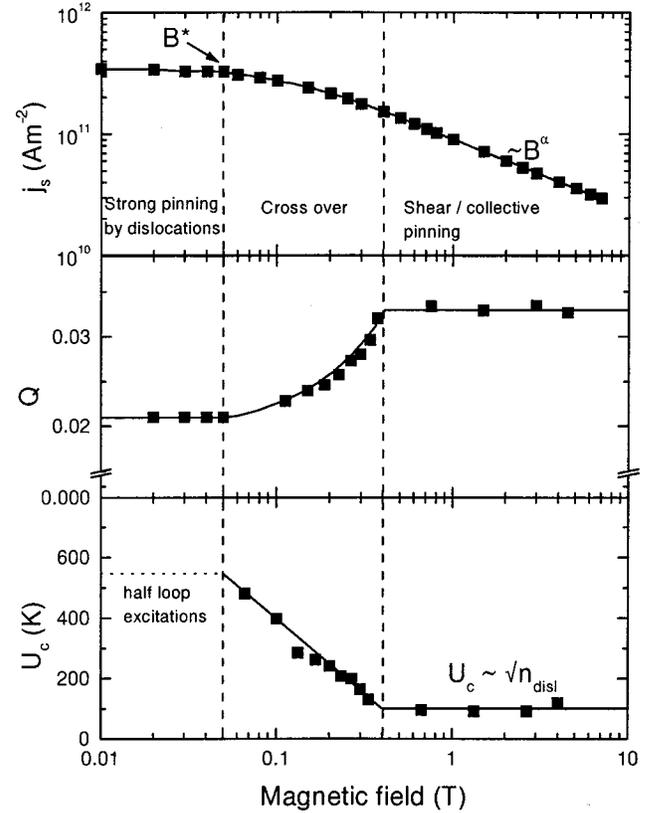

FIG. 16. Different vortex regimes with increasing magnetic field in thin films of YBa$_2$Cu$_3$O$_{7-\delta}$. Three regimes can be clearly distinguished: (i) a strongly pinned vortex lattice below B^*, (ii) a crossover regime, and (iii) a plastic/collective pinning regime at high magnetic fields. Lines are guides to the eye.

perature dependence of the superconducting current density and the relaxation rate, can be described in terms of vortex pinning by growth-induced linear defects. Since the defect size is of the order of ξ and the average defect spacing of the order of λ, columnar defect models have to be adapted accordingly.

In Fig. 16 we give a schematic overview of the typical behavior of $j_s(B)$, $Q(B)$, and $U_c(B)$ in various regimes. At low magnetic fields $\mu_0 H < B^*$ the vortices are strongly pinned by the dislocations resulting in a plateau both in $j_s(B)$ and $Q(B)$. To describe the pinning properties of the linear defects consistently with the Bose glass theory, we derived a generalized expression for $\varepsilon_r(R)$, which is valid for all defect sizes. As a result, we find that the effect of thermal fluctuations is linear with temperature $f(T/\tilde{T}_{dp}^r) \approx 1$ $- T/\tilde{T}_{dp}^r$. Fitting the temperature dependence of $j_c(B=0)$ with the modified expression for $\varepsilon_r(R,T)$ we find a defect size $r_r \approx 1.5-3$ nm $\approx 1-2 \cdot \xi_{ab}(0)$, which corresponds to the estimated core radius of edge and screw dislocations. The elementary excitations in this regime are half-loop excitations, involving a pinning energy of $U_c \approx 600$ K. The temperature dependence of $U_c(T) \sim \xi(T)/\lambda^2(T)$ for half-loop excitations gives a ratio j_s/j_c, in agreement with experiment. However, the strong temperature dependence of the characteristic field remains puzzling. We suspect that $B^*(T)$

is decreased due to the large currents running in the film, resulting in a small activation barrier for vortex jumps. Unfortunately, there is as yet not a model including the effect of the current density on the characteristic field $B^*(T)$.

At intermediate magnetic fields $B^* < \mu_0 H \lesssim 0.5$ T, the critical current density starts to deviate from its plateau value. The relaxation increases, whereas the pinning energy decreases steeply. Since at 0.5 T the inter-vortex spacing equals half the penetration depth, the crossover could mark the onset of a pinning regime where vortex-vortex interactions become increasingly more important.

At high magnetic fields $\mu_0 H \gtrsim 0.5$ T, the superconducting current density decreases as $j_s(B) \sim 1/\sqrt{B}$ for films with low dislocation density $n_{disl} \lesssim 60$ μm^{-2}. The pinning energy is independent of magnetic field, $U_c(B) \simeq 60-200$ K, and it is proportional to $\sqrt{n_{disl}}$. For films with a small defect spacing $d_r < 130$ nm $\approx \lambda$ the current density $j_s(B)$ decreases more strongly with magnetic field, $\alpha = -0.8$ to -1.1. This behavior of α suggests a transition from plastic to collective pinning. The fact, that $U_c(B)$ and the behavior of α depend on the dislocation density, indicates that the linear defects play an important role even far above the matching field.

An important question from an applications point of view is, how to make films with the largest possible current densities at 77 K, and at high magnetic fields. We have seen that especially at elevated temperatures thermal activation causes a large difference between the superconducting current j_s and the critical current j_c. Moreover, the critical current is reduced, as the vortices are pinned only plastically or collectively at high magnetic fields. The results presented in this paper show two possible options to optimize $j_s(B,T)$, namely (i) increasing the *density* of linear pinning sites, and (ii) increasing the *core size* of the linear pinning sites. We will consider here some aspects of both possibilities to achieve higher current densities.

For films with a high n_{disl} the plateau of constant j_s extends up to larger field values, but at high magnetic fields, $\mu_0 H \gg B^*$, $j_s(B)$ decreases faster in these films ($j_s \sim 1/B$ compared to $j_s \sim 1/\sqrt{B}$ for films with a low n_{disl}). Whether increasing the dislocation density also increases j_s(high B) is therefore not *a priori* clear. Moreover, it remains to be seen up to what n_{disl} the plateaulike features in $j_s(B)$ remain intact. We expect that to obtain larger current densities, the nonrandom distribution of natural linear defects is an advantage over the random distribution of columnar tracks, but on the other hand columnar tracks can be produced with far higher densities (several teslas) than natural linear defects ($B_\Phi \sim 200$ mT). Experimentally we find at magnetic fields $\mu_0 H \sim 1-2$ T, that films with many dislocations still carry the largest currents. We conclude that increasing the disloca-

tion density (eventually by heavy ion irradiation) can be effective in achieving higher current densities, but it depends very much on what field and temperature range one is using.

A larger defect size gives a deeper pinning potential and a larger pinning force $f_p = -d\varepsilon_r/dR_{max}$ (cf. Fig. 1). Therefore, increasing the defect size gives intrinsically (i) a larger critical current density j_c [see Eq. (10)] and (ii) a higher pinning energy U_c. Also the temperature dependence $j_c(T) \sim 1/(\lambda^2(T)\xi^\nu(T))$ is less strong for smaller ν, i.e., a larger defect size. From the lines for various ν in Fig. 12 we find at $T = 77$ K, that the critical current density $j_c(\nu=2) \approx 2.5 \cdot j_c(\nu=3)$. The measured critical current density j_s benefits even more from a larger defect size, since the ratio $j_s/j_c \approx 0.2$ (at $T = 77$ K and $\nu = 2$) becomes larger for larger pinning energies, see Eq. (27). Since irradiation by heavy ions produces columnar defects with radius 2-3 times larger than that of linear defects, the reasoning above might explain why irradiation of thin films[28,29,33] is mainly effective in enhancing the critical currents at high ($T = 77$ K) temperatures.[29] In order to increase the diameter of natural linear defects, one would have to find ways to produce (screw) dislocations with Burgers vectors several times the unit cell.

Concluding, we find that the high critical currents in $YBa_2Cu_3O_{7-\delta}$ thin films are to a large extent due to natural linear defects. Due to half loop nucleation vortices can depin rather easily, which reduces the measured current j_s compared to the true critical current density j_c. Theoretically, strong pinning in the high field regime where vortex-vortex interaction competes with vortex pinning still needs to be explored. To obtain the maximum current density at high fields and temperatures, one can either increase the linear defect *density* or the defect *core size*, but at the same time it is important to have a *regular* distribution of linear defects, in order to reduce the effect of vortex-vortex interactions.

APPENDIX A: CALCULATION OF THE VORTEX-PINNING POTENTIAL

To find the pinning potential we integrate Eq. (7) over the full defect

$$\varepsilon_r(R) = -\frac{1}{2}\mu_0 H_c^2 \int_0^{r_r}\int_0^{2\pi}[1-|\Psi(R')|^2]\eta\,d\eta\,d\vartheta, \tag{A1}$$

with $R' = |\mathbf{r} - \mathbf{R}| = r^2 + R^2 - 2rR\cos\vartheta$. Here the origin is at the center of the linear defect, R is the distance from the center of the vortex to the center of the defect, and R' is the distance from the vortex to the point (r,ϑ). With $|\Psi(R')|^2 = R'^2/(R'^2 + 2\xi^2)$ we obtain

$$\varepsilon_r(R) = -\frac{\varepsilon_0}{2\pi} \int_0^{r_r} \int_0^{2\pi} \frac{\eta \, dr \, d\vartheta}{r^2 + R^2 - 2rR \cos\vartheta + 2\xi^2}. \tag{A2}$$

Integrating over ϑ yields

$$\varepsilon_r(R) = -\varepsilon_0 \int_0^{r_r} \frac{r \, dr}{\sqrt{(r^2 + R^2 + 2\xi^2 + 2rR)(r^2 + R^2 + 2\xi^2 - 2rR)}}, \tag{A3}$$

which can be written as

$$\varepsilon_r(R) = -\varepsilon_0 \int_0^{r_r} \frac{r \, dr}{\sqrt{(r^2 - R^2 + 2\xi^2)^2 + 8R^2\xi^2}} \tag{A4}$$

from which we obtain

$$\varepsilon_r(R) = -\frac{\varepsilon_0}{2} \operatorname{arcsinh}\left[\frac{1}{2} \frac{(r^2 - R^2 + 2\xi^2)}{\sqrt{2}\xi|R|}\right]_0^{r_r} \tag{A5}$$

and

$$\varepsilon_r(R) = -\frac{\varepsilon_0}{2} \left\{ \operatorname{arcsinh}\left[\frac{1}{2} \frac{(r_r^2 - R^2 + 2\xi^2)}{\sqrt{2}\xi|R|}\right] - \operatorname{arcsinh}\left[\frac{1}{2} \frac{(-R^2 + 2\xi^2)}{\sqrt{2}\xi|R|}\right] \right\}. \tag{A6}$$

The depth of the pinning potential $\varepsilon_r(0)$ can be calculated straightforwardly from Eq. (A2) by putting in $R=0$. The result is

$$\varepsilon_r(0) = -\frac{\varepsilon_0}{2} \ln\left[1 + \frac{r_r^2}{2\xi^2}\right]. \tag{A7}$$

APPENDIX B: THE EFFECT OF THERMAL FLUCTUATIONS ON THE VORTEX-PINNING POTENTIAL

To calculate the effect of thermal fluctuations on the pinning potential we use the same line of derivation as in Ref. 42. Instead of using a square well potential, we use the Taylor's expansion of Eq. (7):

$$\varepsilon_r(R) \approx \varepsilon_r(R=0) + \frac{\varepsilon_0}{2} \frac{r_r^2}{(r_r^2 + 2\xi^2)^2} R^2 = \varepsilon_r(0) + \frac{1}{2}kR^2 \quad \text{with} \quad k = \frac{\varepsilon_0 r_r^2}{(r_r^2 + 2\xi^2)^2}. \tag{B1}$$

The first term of Eq. (B1) gives the depth of the potential and the second term is a harmonic oscillator potential. The binding energy of a particle trapped in this harmonic oscillator potential in two dimensions is given by

$$E_B = U_0 + \hbar\omega \quad \text{with} \quad \omega = \sqrt{\frac{k}{m}}. \tag{B2}$$

Equation (B2) is translated back to the vortex picture according to the usual mapping $\hbar \to T$, $m \to \varepsilon_l$, $U_0 \to \varepsilon_r(0)$, $\tilde{T}_{dp}^r = b_0 \sqrt{\varepsilon_l \varepsilon_r}$, and k from by Eq. (B1). We obtain for the effective depth of the pinning potential at low temperatures (note that $\varepsilon_r(0) = -1/2\varepsilon_0 \ln[1 + r_r^2/2\xi^2]$ is negative)

$$\varepsilon_r(T) = \varepsilon_r(T=0)\left(1 - \gamma \frac{T}{\tilde{T}_{dp}^r}\right) \quad \text{with} \quad \gamma = \frac{\sqrt{2}x^2}{\sqrt{\ln(1+x^2)}(1+x^2)}. \tag{B3}$$

The prefactor $\gamma \approx 0.85$ for $x>1$ is only weakly dependent of x^2 and we put $\gamma = 1$ and for convenience. Compared to the square well potential the effect of thermal fluctuations changes from $f(T/\tilde{T}_{dp}^r) = 1 - (T/\tilde{T}_{dp}^r)^2$ to $1 - T/\tilde{T}_{dp}^r$. As a result the effective depth of the pinning potential decreases faster with temperature than it was assumed up to now. To obtain the correct temperature dependences for $B^*(T)$ and $j_s(T)$ this extra factor $f(T/\tilde{T}_{dp}^r)$ should be included, together with the temperature dependences for $\xi(T)$ and $\lambda(T)$.

It is obvious that the harmonic oscillator approximation is valid in a limited range $T \ll \tilde{T}_{dp}^r$ only. At high temperatures $T > \tilde{T}_{dp}^r$ it was calculated that $f(T/\tilde{T}_{dp}^r) = \exp(-T/\tilde{T}_{dp}^r)$,[42] at intermediate temperatures $T \lesssim \tilde{T}_{dp}^r$ numerical calculations should be used to obtain an exact result for $f(T/\tilde{T}_{dp}^r)$.

---

[1] T. L. Hylton and M. R. Beasley, Phys. Rev. B **41**, 11 669 (1990).

[2] For an overview of various pinning mechanisms, see, e.g., P. H. Kes, in *Materials and Crystallographic Aspects of HTc-Superconductivity*, edited by E. Kaldis (Kluwer Academic, Dordrecht, 1994), p. 401.

[3] I. Maggio-Aprile, C. Renner, A. Erb, E. Walker, and Ø Fischer, Nature (London) **390**, 487 (1997).

[4] A. Gurevich and L. D. Cooley, Phys. Rev. B **50**, 13 563 (1994).

[5] M. Murakami, M. Morita, K. Doi, and K. Miyamoto, Jpn. J. Appl. Phys., Part 1 **28**, 1189 (1989).

[6] H. Douwes, P. H. Kes, Ch. Gerber, and J. Mannhart, Cryogenics **33**, 486 (1993).

[7] Ch. Jooss, A. Forkl, R. Warthmann, H.-U. Habermeier, B. Leibold, and H. Kronmüller, Physica C **266**, 235 (1996); Ch. Jooss, A. Forkl, and H. Kronmüller, *ibid.* **268**, 87 (1996).

[8] E. Sheriff, R. Prozorov, Y. Yeshurun, A. Shaulov, G. Koren, and C. Chabaud-Villard, J. Appl. Phys. **82**, 4417 (1997).

[9] M. Hawley, I. D. Raistrick, J. G. Beery, and R. J. Houlton, Science **251**, 1587 (1991).

[10] J. Mannhart, D. Anselmetti, J. G. Bednorz, A. Catana, Ch. Gerber, K. A. Müller, and D. G. Schlomm, Z. Phys. B: Condens. Matter **86**, 177 (1992).

[11] H. Douwes and P. H. Kes, J. Alloys Compd. **195**, 451 (1993).

[12] V. M. Pan, A. L. Kasatkin, V. L. Svetchnikov, and H. W. Zandbergen, Cryogenics **33**, 21 (1993).

[13] X. Y. Cai, A. Gurevich, I-Fei Tsu, D. L. Kaiser, S. E. Babcock, and D. C. Larbalestier, Phys. Rev. B **57**, 10 951 (1998).

[14] A. Díaz, L. Mechin, P. Berghuis, and J. E. Evetts, Phys. Rev. Lett. **80**, 3855 (1998).

[15] Ch. Jooss, R. Warthmann, H. Kronmüller, T. Haage, H.-U. Habermeier, and J. Zegenhagen, Phys. Rev. Lett. **82**, 632 (1999); Ch. Jooss, R. Warthmann, and H. Kronmüller, Phys. Rev. B **61**, 12 433 (2000).

[16] L. Civale, A. D. Marwick, T. K. Worthington, M. A. Kirk, J. R. Thompson, L. Krusin-Elbaum, Y. Sun, J. R. Clem, and F. Holtzberg, Phys. Rev. Lett. **67**, 648 (1991).

[17] M. Konczykowski, F. Rullier-Albenque, E. R. Yacoby, A. Shaulov, Y. Yeshurun, and P. Lejay, Phys. Rev. B **44**, 7167 (1991).

[18] W. Gerhäuser, G. Ries, H. W. Neumüller, W. Schmidt, O. Eibl, G. Saemann-Ischenko, and S. Klaumünzer, Phys. Rev. Lett. **68**, 879 (1992).

[19] V. V. Moshchalkov, M. Baert, V. V. Metlushko, E. Rosseel, M. J. van Bael, K. Temst, R. Jonckheere, and Y. Bruynseraede, Phys. Rev. B **54**, 7385 (1996).

[20] A. Castellanos, R. Wördenweber, G. Ockenfuss, A. VonderHart, and K. Keck, Appl. Phys. Lett. **71**, 962 (1997).

[21] L. M. Paulius, C. C. Almasan, and M. B. Maple, Phys. Rev. B **47**, 11 627 (1993).

[22] H. H. Wen, Z. X. Zhao, Y. G. Xiao, B. Yin, and J. W. Li, Physica C **251**, 371 (1995).

[23] D. N. Zheng, A. M. Campbell, J. D. Johnson, J. R. Cooper, F. J. Blunt, A. Porch, and P. A. Freeman, Phys. Rev. B **49**, 1417 (1994).

[24] R. Noetzel and K. Westerholt, Phys. Rev. B **58**, 15 108 (1998).

[25] G. Hammerl, A. Schmehl, R. R. Schulz, B. Goetz, H. Bielefeldt, C. W. Schneider, H. Hilgenkamp, and J. Mannhart, Nature (London) **407**, 162 (2000); A. Schmehl, B. Goetz, R. R. Schulz, C. W. Schneider, H. Bielefeldt, H. Hilgenkamp, and J. Mannhart, Europhys. Lett. **47**, 110 (1999).

[26] L. Civale, Supercond. Sci. Technol. **10**, A11 (1997), and references therein.

[27] D. R. Nelson and V. M. Vinokur, Phys. Rev. B **48**, 13 060 (1993).

[28] B. Roas, B. Hensel, G. Saemann-Ischenko, and L. Schultz, Appl. Phys. Lett. **54**, 1051 (1989); B. Roas, B. Hensel, S. Henke, S. Klaumünzer, B. Kabius, W. Watanabe, G. Saemann-Ischenko, L. Schultz, and K. Urban, Europhys. Lett. **11**, 669 (1990).

[29] M. P. Siegal, R. B. Vandover, J. M. Phillips, E. M. Gyorgy, A. E. White, and J. H. Marshall, Appl. Phys. Lett. **60**, 2932 (1992).

[30] Th. Schuster, H. Kuhn, M. R. Koblischka, H. Theuss, H. Kronmüller, M. Leghissa, M. Kraus, and G. Saemann-Ischenko, Phys. Rev. B **47**, 373 (1993).

[31] C. Gerber, D. Anselmetti, J. G. Bednorz, J. Mannhart, and D. G. Schlom, Nature (London) **350**, 279 (1991).

[32] B. Dam, J. H. Rector, J. M. Huijbregtse, and R. Griessen, Physica C **305**, 1 (1998).

[33] E. Mezzetti, R. Gerbaldo, G. Ghigo, L. Gozzelino, B. Minetti, C. Camerlingo, A. Monaco, G. Cuttone, and A. Rovelli, Phys. Rev. B **60**, 7623 (1999); G. Ghigo, A. Chiodoni, R. Gerbaldo, L. Gozzelino, E. Mezzetti, B. Minetti, C. Camerlingo, G. Cuttone, and A. Rovelli, Supercond. Sci. Technol. **12**, 1059 (1999); E. Mezzetti, A. Chiodoni, R. Gerbaldo, G. Ghigo, L. Gozzelino, B. Minetti, C. Camerlingo, and A. Monaco, Physica C **332**, 115 (2000).

[34] B. Dam, J. M. Huijbregtse, F. C. Klaassen, R. C. F. van der Geest, G. Doornhos, J. H. Rector, A. M. Testa, S. Freisem, J. C. Martínez, B. Stäuble-Pümpin, and R. Griessen, Nature (London) **399**, 439 (1999).

[35] R. H. Koch, V. Foglietti, W. J. Gallagher, G. Koren, A. Gupta, and M. P. A. Fischer, Phys. Rev. Lett. **63**, 1511 (1989).

[36] D. S. Fisher, M. P. A. Fisher, and D. A. Huse, Phys. Rev. B **43**, 130 (1991).

[37] G. W. Crabtree, W. K. Kwok, U. Welp, D. Lopez, and J. A. Fendrich, in *Physics and Materials Science of Vortex States, Flux Pinning and Dynamics*, Vol. 356 of *NATO Advanced Study Institute, Senes E: Applied Sciences*, edited by R. Kossowsky *et al.* (Plenum, New York, 1999), p. 357 and references therein.

[38] I. A. Larkin and Yu. N. Ovchinnikov, J. Low Temp. Phys. **34**, 409 (1979).

[39] G. Blatter, M. V. Feigel'man, V. B. Geshkenbein, A. I. Larkin, and V. M. Vinokur, Rev. Mod. Phys. **66**, 1125 (1994).

[40] G. S. Mkrtchyan and V. V. Shmidt, Sov. Phys. JETP **34**, 195 (1972).

[41] D. R. Nelson and V. M. Vinokur, Phys. Rev. Lett. **68**, 2398 (1992).

[42] Blatter *et al.* (Ref. 39), p. 1327 and further.

[43] In the review by Blatter *et al.* (Ref. 39) the symbol B_{rb} is used for the crossover or accommodation field. We will use B^* throughout this paper like in Ref. 34, but for all other symbols we use the notation used in Ref. 39.

[44] J. M. Huijbregtse, B. Dam, R. C. F. van der Geest, F. C. Klaassen, R. Elberse, J. H. Rector, and R. Griessen, Phys. Rev. B **62**, 1338 (2000).

[45] L. Krusin-Elbaum, L. Civale, J. R. Thompson, and C. Feild, Phys. Rev. B **53**, 11 744 (1996).

[46] J. R. Clem, J. Low Temp. Phys. **18**, 427 (1975).

[47] J. M. Huijbregtse, B. Dam, J. H. Rector, and R. Griessen, J. Appl. Phys. **86**, 6528 (1999).

[48] The average transition temperature and transition width were determined by measuring a large collection of $YBa_2Cu_3O_{7-\delta}$ films (see Ref. 47), including the films listed in Table I.

[49] M. T. Pannetier, F. C. Klaassen, R. J. Wijngaarden, M. Welling, K. Heeck, J. M. Huijbregtse, B. Dam, and R. Griessen, Phys. Rev. B **64**, 144505 (2001).

[50] S. Freisem, A. Brockhoff, D. G. de Groot, B. Dam, and J. Aarts, J. Magn. Magn. Mater. **165**, 380 (1997).

[51] J. C. Martínez, B. Dam, B. Stäuble-Pümpin, G. Doornbos, R. Surdeanu, U. Poppe, and R. Griessen, J. Low Temp. Phys. **105**, 1017 (1996).

[52] B. Dam, C. Træholt, B. Stäuble-Pümpin, J. Rector, and D. G. de Groot, J. Alloys Compd. **251**, 27 (1997).

[53] J. M. Huijbregtse, F. C. Klaassen, A. Szepielow, J. H. Rector, B. Dam, R. Griessen, B. J. Kooi, and J. Th. M. de Hosson (unpublished).

[54] A. Gurevich and E. A. Pashitskii, Phys. Rev. B **57**, 13 878 (1998).

[55] N. F. Heinig, R. D. Redwing, I. Fei Tsu, A. Gurevich, J. E. Nordman, S. E. Babcock, and D. C. Larbalestier, Appl. Phys. Lett. **69**, 577 (1996).

[56] C. P. Bean, Phys. Rev. Lett. **8**, 250 (1962).

[57] E. H. Brandt, Phys. Rev. B **48**, 6699 (1993).

[58] M. V. Indenbom, C. J. van der Beek, M. Konczykowski, and F. Holtzberg, Phys. Rev. Lett. **84**, 1792 (2000).

[59] M. Qvarford, K. Heeck, J. G. Lensink, R. J. Wijngaarden, and R. Griessen, Rev. Sci. Instrum. **63**, 5726 (1992).

[60] Y. Yeshurun and A. P. Malozemoff, Phys. Rev. Lett. **60**, 2202 (1988).

[61] A. C. Mota, A. Pollini, P. Visani, K. A. Müller, and J. G. Bednorz, Phys. Rev. B **36**, 4011 (1987).

[62] G. Doornbos, Ph.D. thesis, Vrije Universiteit, 2001.

[63] A. J. J. van Dalen, M. R. Koblischka, and R. Griessen, Physica C **259**, 157 (1996).

[64] M. Däumling and D. C. Larbalestier, Phys. Rev. B **40**, 9350 (1989).

[65] L. W. Conner and A. P. Malozemoff, Phys. Rev. B **43**, 402 (1991).

[66] R. Wördenweber, Phys. Rev. B **46**, 3076 (1992); Cryogenics **32**, 1098 (1992).

[67] H. Schnack, R. Griessen, J. G. Lensink, and H. H. Wen, Phys. Rev. B **48**, 13 178 (1993).

[68] A. P. Malozemoff and M. P. A. Fischer, Phys. Rev. B **42**, 6784 (1990); see also H. H. Wen, Z. X. Zhao, R. J. Wijngaarden, J. H. Rector, B. Dam, and R. Griessen, *ibid.* **52**, 4583 (1995).

[69] I. L. Landau and H. R. Ott, Physica C **340**, 251 (2000); J. Chen, D. L. Yin, P. Zheng, J. Hammann, G. C. Xiong, Q. Jiang, K. Wu, Z. J. Chen, and D. Jin, *ibid.* **282−287**, 2267 (1997).

[70] A. F. Th. Hoekstra, A. M. Testa, G. Doornbos, J. C. Martínez, B. Dam, R. Griessen, B. I. Ivlev, M. Brinkmann, K. Westerholt, W. K. Kwok, and G. W. Crabtree, Phys. Rev. B **59**, 7222 (1999).

[71] M. V. Feigel'man, V. B. Geshkenbein, A. I. Larkin, and V. M. Vinokur, Phys. Rev. Lett. **63**, 2303 (1989); M. V. Feigel'man, V. B. Geshkenbein, and V. M. Vinokur, Phys. Rev. B **43**, 6263 (1991).

[72] B. Holzapfel, G. Kreiselmeyer, M. Kraus, G. Saemann-Ischenko, S. Bouffard, S. Klaumünzer, and L. Schultz, Phys. Rev. B **48**, 600 (1993).

[73] R. Prozorov, A. Tsameret, Y. Yeshurun, G. Koren, M. Konczykowski, and S. Bouffard, Physica C **234**, 311 (1994).

[74] G. Nakielski, A. Rickertsen, T. Steinborn, J. Wiesner, G. Wirth, A. G. M. Jansen, and J. Kötzler, Phys. Rev. Lett. **76**, 2567 (1996).

[75] T. Sueyoshi, N. Ishikawa, A. Iwase, Y. Chimi, T. Kiss, T. Fujiyoshi, and K. Miyahara, Physica C **309**, 79 (1998).

[76] B. Roas, L. Schultz, and G. Saemann-Ischenko, Phys. Rev. Lett. **64**, 479 (1990).

[77] The value for C can be determined independently as it is given by $C = -\lim_{T\to 0}(1/Q)(d\ln j_s/d\ln T)$. The values $C=15$ and $C=19$ were obtained for $A67$ and $F554$, respectively.

[78] Y. Gao, K. L. Merkle, G. Bai, H. L. M. Chang, and D. J. Lam, Physica C **174**, 1 (1991).

[79] J. R. Thompson, L. Krusin-Elbaum, L. Civale, G. Blatter, and C. Feild, Phys. Rev. Lett. **78**, 3181 (1997).

[80] Hereby we neglect the field dependence of μ. We assume that, as we are in a specific pinning regime, μ is independent of B. This assumption is strictly speaking not true, but to obtain a crude estimate it is sufficient.

[81] A. Schönenberger, A. Larkin, E. Heeb, V. Geshkenbein, and G. Blatter, Phys. Rev. Lett. **77**, 4636 (1996).

[82] A. F. Th. Hoekstra, R. Griessen, A. M. Testa, J. el Fattahi, M. Brinkmann, K. Westerholt, W. K. Kwok, and G. W. Crabtree, Phys. Rev. Lett. **80**, 4293 (1998).

[83] R. A. Doyle, W. S. Seow, J. D. Johnson, A. M. Campbell, P. Berghuis, R. E. Somekh, J. E. Evetts, G. Wirth, and J. Wiesner, Phys. Rev. B **51**, 12 763 (1995).